galaxies

MDPI

Article

The Interstellar Medium of Dwarf Galaxies

Christian Henkel [1,2,3,*], Leslie K. Hunt [4] and Yuri I. Izotov [5]

[1] Max-Planck-Institut für Radioastronomie, Auf dem Hügel 69, 53125 Bonn, Germany
[2] Department of Astronomy, Faculty of Science, King Abdulaziz University, P.O. Box 80203, Jeddah 21589, Saudi Arabia
[3] Xinjiang Astronomical Observatory, Chinese Academy of Sciences, Urumqi 830011, China
[4] INAF—Osservatorio Astrofisico di Arcetri, Largo E. Fermi, 5, 50125 Firenze, Italy; leslie.hunt@inaf.it
[5] Bogolyubov Institute for Theoretical Physics, National Academy of Sciences of Ukraine, 14-b Metrolohichna Str., UA-03143 Kyiv, Ukraine; yizotov@bitp.kiev.ua
* Correspondence: chenkel@mpifr-bonn.mpg.de

Abstract: Dwarf galaxies are by far the most numerous galaxies in the Universe, showing properties that are quite different from those of their larger and more luminous cousins. This review focuses on the physical and chemical properties of the interstellar medium of those dwarfs that are known to host significant amounts of gas and dust. The neutral and ionized gas components and the impact of the dust will be discussed, as well as first indications for the existence of active nuclei in these sources. Cosmological implications are also addressed, considering the primordial helium abundance and the similarity of local Green Pea galaxies with young, sometimes protogalactic sources in the early Universe.

Keywords: dwarf galaxies; irregular galaxies; blue compact galaxies; green peas; super star clusters

check for updates

Citation: Henkel, C.; Hunt, L.K.; Izotov, Y.I. The Interstellar Medium of Dwarf Galaxies. *Galaxies* **2022**, *10*, 11. https://doi.org/10.3390/galaxies10010011

Academic Editor: Michele Bellazzini

Received: 6 October 2021
Accepted: 6 December 2021
Published: 12 January 2022

Publisher's Note: MDPI stays neutral with regard to jurisdictional claims in published maps and institutional affiliations.

Copyright: © 2022 by the authors. Licensee MDPI, Basel, Switzerland. This article is an open access article distributed under the terms and conditions of the Creative Commons Attribution (CC BY) license (https://creativecommons.org/licenses/by/4.0/).

1. Introduction

Luminous massive stars are rare and experience a remarkable but short lifetime. Low mass stars, even though occasionally flaring, are much less conspicuous but are numerous, and have lifetimes that usually exceed a Hubble time; they are also able to conserve much of their original composition. Galaxies are, in some respect, qualitatively similar. The most massive ones are also rare and luminous. After a relatively brief active phase they tend to become quiescent giant ellipticals, 'cD' or 'D' galaxies, exhibiting (if at all) only little star formation during the current epoch. Small galaxies, like their low mass stellar cousins, dominate not only in number (e.g., [1–3]) but can also retain in many cases significant amounts of their original elemental composition, eventually even re-activating larger galaxies through minor mergers. In exceptional cases they can stay isolated up to the present day. Dwarf galaxies are therefore of high importance not only in their own right: because of their physical, chemical and kinematical properties they also serve as proxies of the distant, early and chemically-unevolved Universe. Furthermore, their spatial distribution helps to constrain models of the evolution of the Universe. Thus dwarf galaxies are not only relevant for a better understanding of our 'neighborhood', addressing ongoing local physical, chemical and dynamical processes, but they also have the potential to shed light onto the distant past with otherwise inaccessible linear resolution.

The generally accepted rule to define the term 'dwarf galaxy' is based on luminosity rather than size. Clearly, dwarfs must be small and dim with respect to Milky Way sized major galaxies and bright and extended with respect to old globular clusters like those encountered in the Galaxy. Small galaxies are often irregularly shaped and sometimes severely stretched by interactions. Therefore luminosity, not size, is commonly chosen as a criterion to identify dwarf galaxies. In case of a low level of obscuration by dust (see below), this is also an indicator of mass even though mass-to-luminosity ratios may vary substantially in view of the presence or absence of young massive stars (e.g., [4]). In the

following we consider an upper luminosity bound of $M_V \approx -18^M$ ($L_V \approx 1.4 \times 10^9\,L_{V,\odot}$), unless otherwise noted. This implies that the bulk of galaxies being able to form spiral disks are not included. Galaxies like the Large Magellanic Cloud (LMC) and the Triangulum galaxy (M 33) in the local and M 82 in in the nearby ($D \approx 3.5$ Mpc) M 81 group are slightly too luminous. However, the Small Magellanic Cloud (SMC) lies well below the above mentioned upper luminosity threshold. At the lower end, we assume that a dwarf galaxy with a well developed stellar component must be significantly more luminous than a typical globular cluster in the Milky Way. This implies $M_V \ll -8^M$ (for dwarfs with an even lower stellar luminosity, being almost always devoid of a notable interstellar medium, see [5]). Massive objects mainly consisting of neutral hydrogen and lacking a significant stellar component appear to be statistically irrelevant ([6]; see also Section 4.3), while (damped) Ly-α systems are beyond the scope of this paper.

In Section 2, we describe the main classes of dwarf galaxies and their characteristics. The main components of their interstellar medium are introduced in Section 3. An overview of the interplay of these different components, modes of star formation and the presence of active galactic nuclei are the topic of Section 4. Section 5 introduces individual star-forming dwarfs in the local Universe, while some cosmological aspects are discussed in Section 6. Finally, attractive future prospects and promising avenues for future research are summarized in Section 7.

2. Dwarf Galaxies: General Properties

2.1. Morphological Types

Prior to a detailed analysis of the interstellar medium (ISM) of dwarf galaxies, we first have to address their heterogeneity. Dwarf ellipticals (dEs), a prominent group among early-type galaxies, populate like their more massive cousins a 'fundamental plane' in three dimensional space, defined by the central projected velocity dispersion, a linear scale (e.g., the 'core', 'half-light' or 'effective' radius) and a surface brightness (averaged over the core, half-light or effective radius). Nevertheless they are quite distinct from giant ellipticals, since they become more diffuse with decreasing luminosity and do not follow the de Vaucouleurs $r^{1/4}$ but more closely an exponential light distribution. Furthermore, these smaller galaxies do not occupy the same fundamental plane and show a larger scatter in their parameters (e.g., [7,8]) due to variations in the mass-to-luminosity ratios and structural parameters. The morphological transition from E to dE is near $M_B = -18^M$, but there is overlap. M32, the compact satellite of the Andromeda nebula M31, still follows the de Vaucouleurs law (e.g., [9]). Some dS0 galaxies also exist, which, below, will be lumped together with the dE objects. Many of the more luminous dEs ($M_B \lesssim -16^M$) are 'nucleated', possessing a central star cluster sometimes reaching $M_V = -12^M$ (see e.g., NGC 205 in Section 5.2). Some of these galaxies also show evidence for the existence of disks and spiral structure and bars (e.g., [10–12]). While some of the dEs appear to be rotationally supported, others appear to be pressure supported and there are cases with kinematically decoupled cores (e.g., [13,14]).

In our Local Group, dwarf spheroidal galaxies (dSphs) are numerous. Being much more extended than globular clusters, they are faint, difficult to find, commonly lack a detectable interstellar medium and are therefore not a major topic of this review. Typically, they did not form stars since several hundred million years or more (e.g., [15]). A lack of a notable interstellar medium also characterizes the even less luminous ultra-diffuse galaxies (UDGs) and ultra-faint dwarfs (UFDs) at $M_V \gtrsim -7.7^M$ ($L \lesssim 10^5\,L_\odot$; [5]) as well as the ultra-compact dwarfs, the latter with structural properties that resemble those of ω Cen (e.g., [5,15,16]).

There are not only 'early-type' but also 'late-type' galaxies of low luminosity, often following an exponential surface brightness profile. These are commonly termed dwarf irregular galaxies (dIrrs) with the Small Magellanic Cloud (SMC) and NGC 6822 as the nearest such objects. Some of them, like the SMC, owe their shape to a recent interaction with another galaxy. The majority of this class of objects is characterized by a massive

interstellar medium that is dominated by neutral hydrogen (HI; see e.g., [17]). Among this class of late-type objects, blue compact dwarf galaxies (BCDs) stand out because they host sites of recent or ongoing massive star formation,[1] by a high surface brightness, e.g., $\mu_{B,peak} < 22^m/arcsec^2$, and blue color, e.g., $\mu_{B,peak} - \mu_{R,peak} \lesssim 1^m$. Even more active but sometimes showing luminosities exceeding our definition of a dwarf galaxy (Section 1) are the 'Green Peas' (also termed Luminous Compact Galaxies, LCGs), compact metal poor galaxies of size ≈5 kpc or less, that are vigorously forming stars (e.g., [18]). Their color is related to intense emission in the [OIII]λ5007 line and is particularly dominant at optical wavelengths, when redshifts move the Hα line out of the optical spectral window. Naturally, the green color refers to those galaxies detected at moderate redshifts ($z \approx 0.2$) and changes at lower and higher redshifts.

It is sometimes difficult to distinguish quiescent dIrr galaxies from their dE counterparts. Furthermore, there exist real transitory objects, like the Phoenix system (e.g., [9]). Early-type dwarfs can be former late-type systems that have lost their gas in a crowded environment (e.g., [19,20]). While the Local Group contains several dIrr galaxies, BCDs are rarer and only a single such object, IC 10, has been suggested to be located within its volume [21]. Green peas are even rarer than BCDs and are therefore commonly observed at redshifts $z > 0.1$. Not surprisingly, dIrrs preferentially reside in field environments, while dEs are more commonly found in denser more clustered regions (e.g., [15,17]; for the Virgo cluster, see e.g., [22]). The latter also holds for the relatively luminous nucleated dwarfs.

2.2. Physical and Chemical Boundary Conditions

As a start, we have to mention basic differences between the ISM of dwarfs and giant galaxies. For dwarfs:

- The ISM is metal poor.
- Gravity is weak.
- Interstellar pressure is low.
- As a consequence, disks tend to be thick and diffuse.
- Low gravity and pressure may lead to strong feedback effects.
- There is little shear due to rotational effects.
- There is no high-contrast spiral structure shocking and compressing the gas.
- Dust to gas mass ratios (M_d/M_g) are low.
- Insufficient dust shielding leads to a harsh environment for molecular species.
- Low M_d/M_g ratios lead to a low gas phase depletion of refractory elements onto dust grains.

For mass-metallicity and luminosity-metallicity correlations (Figure 1), metallicities are mainly deduced from optical spectra of HII regions, see e.g., [23–26]. Because of their small masses, rotation speeds in dwarfs are low, far below $v_{rot} = 100\,km\,s^{-1}$, which implies that random dynamical events can play a significant role in shaping the detailed velocity field. Late-type dwarf irregulars tend to show rotation, even though sometimes with very low rates ($v_{rot}/\sigma < 1$; σ: velocity dispersion; e.g., [27])). On the other hand, it is hard to find rotating dwarf spheroidals. This also holds for the larger dwarf ellipticals NGC 147, NGC 185, and NGC 205 that accompany the Andromeda nebula (e.g., [15,28]). A deeper consideration of rotational properties would require a discussion of dark matter and alternative gravitational theories, which is the topic of accompanying articles and therefore beyond the scope of this work. This also holds for a detailed discussion of the Tully-Fisher relation. Here we focus instead on directly observable ISM properties, starting with the most extended and also by mass most dominant interstellar component, the atomic hydrogen (HI). This is followed by discussions of the the dust and molecular gas components to then also address relevant properties of the ionized medium. Not mentioned below but also relevant for this study is that we assume a solar system metallicity of $Z = 12 + \log(O/H) = 8.7$ to 8.9 [29] and that in small galaxies showing little nuclear processing carbon and nitrogen tend to be even more depleted than oxygen (e.g., [30–32]).

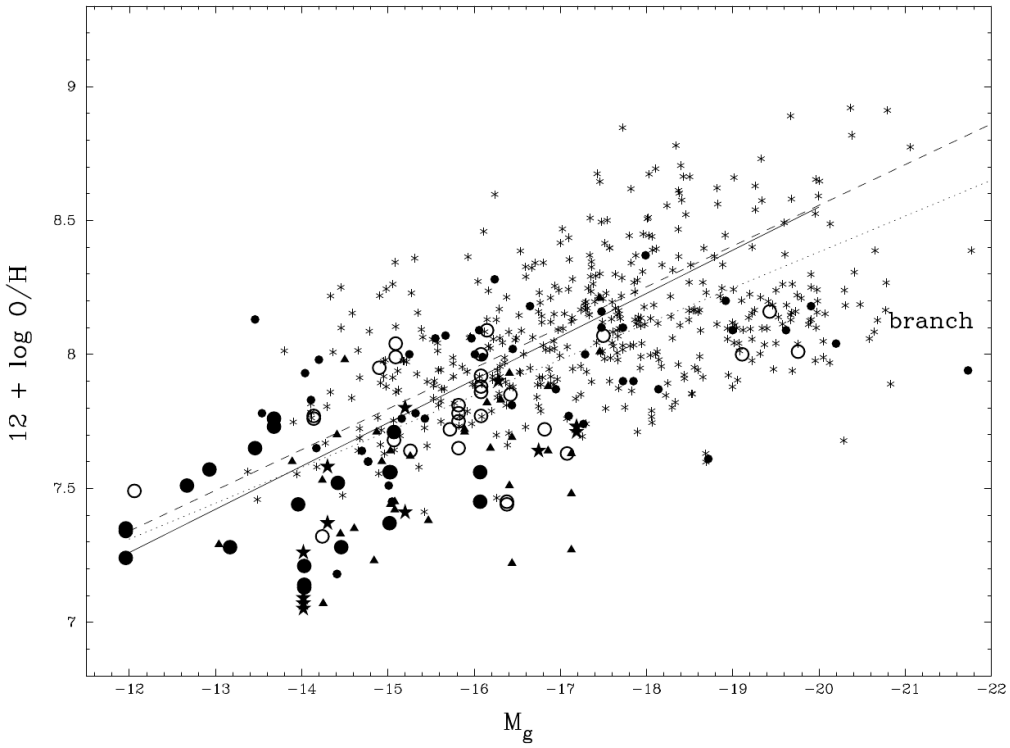

Figure 1. Oxygen abundances of mostly local galaxies as a function of absolute g-magnitude. 'Branch' on the right hand side indicates particularly distant objects ($z > 0.2$). Small filled circles: data from [33,34]; large filled circles: data from [35]; asterisks: a Sloan Digital Sky Survey (SDSS) sample; open circles: 3.6 m ESO data; stars: VLT data; triangles: additional VLT data from [36]. For more details, see [23].

3. Main Components of the Interstellar Medium

3.1. Neutral Hydrogen (HI)

Several large surveys of the $\lambda \approx 21$ cm line, with arcsecond resolution and channel widths of only a few km s^{-1}, have been carried out to unveil the properties of HI in galaxies of low luminosity. Over the last 10 to 15 years, the most important of these include FIGGS (Faint Irregular Galaxies GMRT Survey; [37]) with the Giant Meter Radio Telescope covering ≈60 nearby ($D \lesssim 4$ Mpc) dwarfs and the *JVLA* (*Jansky Very Large Array*) projects THINGS (The HI Nearby Galaxy Survey; [38]) with 12 dwarfs among the 34 targeted sources, SHIELD (Survey of HI in Extremely Low mass Dwarfs; [39]) with 12 sources, and the *JVLA*-ANGST survey (Very Large Array survey of ACS Nearby Galaxy Survey Treasury galaxies; [40]) encompassing 35 dwarfs at $D \lesssim 4$ Mpc. The Little Things survey (Local Irregulars That Trace Luminosity Extremes; [41]), again obtained with the *JVLA*, presents observations of 37 dwarf irregulars and 4 BCDs, while a compilation of local volume objects (distance $D < 11$ Mpc), comprising a total of 1072 galaxies, among them many dwarfs, has been presented by [17].

Among these 1072 nearby galaxies, 52% are late-type and 34% early-type dwarfs, amounting to more than 80% of the sample. Half of these are located near major galaxies like the Milky Way or M 81. While spheroidal dwarfs show a tendency to be located in more crowded environments, there also exist rare exceptions from this rule with dSphs quite far from any major source, but being nevertheless devoid of a significant interstellar medium [17]. HI is detected in 91% (424/467) of the HI observed late-type but only in 7% (13/180) of the HI observed early-type dwarfs. Plotting exclusively late type galaxies (T = 5–10, following the revised Hubble system), the HI to stellar mass ratio (M(HI)/M_*; see Figure 2) is to first order constant and close to unity. While not unexpectedly decreasing to values well below unity in massive galaxies, a large scatter would also be introduced if values far below unity would be included from dSph and dE galaxies at the low mass end.

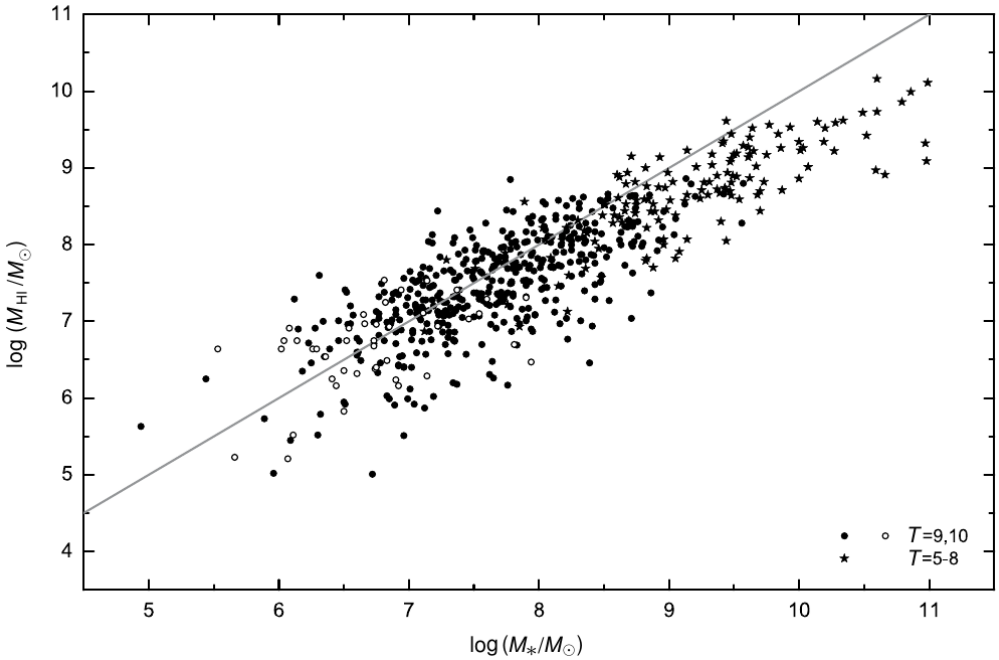

Figure 2. Neutral hydrogen versus stellar masses of late-type galaxies (T = 5–10) in the local volume ($D < 11$ Mpc). Open circles denote galaxies with upper HI flux limits. The solid line connects points with equal HI and stellar masses from [17].

JVLA observations of the BCD Haro 11 [42] showed an intriguing result where no emission but rather absorption has been detected towards the center of the continuum emission including the location of the so-called knot B. Possibly, this is the first dwarf galaxy showing HI absorption against its own central continuum emission, reminiscent of a situation commonly encountered in radio galaxies (e.g., [43]). To discuss larger samples, Ref. [44] measured with the Green Bank 100 m telescope 29 galaxies with 12 + log(O/H) $\leq$ 7.6 and obtained detections in almost all of them (28/29). They find an increasing gas mass fraction with decreasing luminosity, mass and metallicity, dominated by HI. Ref. [45] analyzed within the framework of the Little Things project the HI emission of three seemingly isolated BCDs to find out what is triggering their enhanced star formation activity. An obvious interaction with other sources is not found, but advanced mergers, strong stellar feedback and/or ram pressure stripping might be viable possibilities.

A first HI survey of Green Pea galaxies at redshifts <0.1 was recently published by [46]. For the detected 19 sources (a 50% detection rate) the M(HI)/M_* mass ratios are quite high and consistent with expectations for such active compact dwarf galaxies (see Figure 2). However, the atomic gas depletion timescale is extremely short, with τ_{dep} = M(HI)/SFR $\approx$ 0.6 Gyr (SFR denotes the star-forming rate). This is only about 10% of the commonly attained values by main sequence galaxies showing standard specific star formation rates (sSFR = SFR/M_*).

3.2. The Dust Component

The *InfraRed Astronomical Satellite* (*IRAS*) with wavelengths of 12.5–100 μm, the *Infrared Space Observatory* (*ISO*) at 2.5–240 μm, and the *Spitzer* mission (3.6–180 μm) provided fundamental insights into the extragalactic infrared (IR) sky, revealing galaxies that are emitting electromagnetic radiation almost exclusively in the infrared. However, while these observatories had apertures of 57, 60 and 85 cm, respectively, it is the *Herschel Space Observatory* with its superior 3.5 m mirror that provided more recently, from 2009 to 2013, the deepest infrared views into space with a wavelength range of 70–500 μm. While dust is, even compared with the gas, only a tiny component by mass, it dominates the infrared emission and is an essential ingredient to soften radiation emitted at higher frequencies through

absorption and re-emission, to protect molecules from photodissociation (Section 3.4), and to provide appropriate cooling for an ISM mainly heated by stellar activity.

Dust grains require metals to form (e.g., [47]). These are synthesized in stars, being released into the ISM either on short time scales by supernovae or on longer time scales during the asymptotic giant branch phase of stars with lower mass ($M < 8\,M_{\odot}$). Dust is accumulated during quiescent phases in well shielded regions and processed in harsher environments, including energetic stellar radiation, shocks and stellar or galactic winds. At very low metallicities of 12 + log(O/H) < 8.0, dust grains are difficult to form due to the harsh conditions in an almost unshielded ISM. Only at higher metallicities the fractional interstellar dust grain abundance can grow approximately proportionally to the fractional oxygen abundance (e.g., [48,49]). At lower metallicities, the dust-to-gas mass ratio tends to decrease faster than the oxygen abundance (see also the model calculations of [50]) but there may be exceptions [51,52].

It was early recognized that dwarf galaxies host hotter dust but less emission from so-called polyaromatic hydrocarbons (PAHs) with their numerous bands in the mid-infrared, the most prominent of them located at 6.2, 7.7, 8.6, 11.3 and 12.7 μm. There is a gradual decrease in PAH emission with decreasing metallicity, while the far-infrared color temperature of the large dust grains reaches a peak near 12 + log(O/H) = 8.0 (e.g., [48,53,54]). 50 local dwarf galaxies were studied by the *Herschel* Dwarf Galaxy Survey and compared with dust properties of larger galaxies [55–57]. A characteristic long wavelength ($\lambda > 20$ μm) emissivity-index of $\beta_{\rm IR} = -1.7$ was obtained, that does not strongly depend on metallicity ($\beta_{\rm IR}$ is defined by $S = \nu^{\beta_{\rm IR}} \times B(\nu, T_{\rm dust})$ with S denoting the flux density, ν the frequency, and B representing the Planck function). Because of higher temperatures, for dwarfs the dust emission per mass unit can be several times stronger in the FIR/submm bands than in galaxies of approximately solar metallicity. The dust morphology is clumpy, and in dwarfs mainly heated by massive stars (e.g., [47]). In cases of high Hβ equivalent widths and luminosities, there can be dust components that reach, based on *WISE (Wide-field Infrared Survey Explorer)* temperatures of several 100 K ([58]; for an individual source, see also [59]).

Dust obscures emission at wavelengths shorter than the size of the grains, thus can affect fundamental parameters obtained at near infrared, optical and UV wavelengths. However, the effect appears not to be large in most sources. Internal extinction is apparently insignificant in most dwarf galaxies (e.g., [32]), while [58] find a total (Galactic extinction plus the intrinsic extinction of the extragalactic object) of $A_{\rm V} = 0\overset{\rm m}{.}6$ as a typical value for their large sample of ≈14,000 SDSS (Sloan Digital Sky Survey) galaxies with an average oxygen abundance of 12 + log(O/H) = 7.95. Although optical recombination lines tend to give fairly low values of $A_{\rm V}$ in dwarf galaxies, near- and mid- infrared recombination lines give much higher values (e.g., [32,60,61]) implying that at least some dwarfs host dust-embedded HII regions despite their low metallicity.

3.3. The Submillimeter Excess

At $\gtrsim$500 μm, continuum levels are obtained that surpasss expected flux densities deduced from the measured dust emission obtained at shorter wavelengths by significant >10%. To give an example: 41% of the 22 targets of the *Herschel* Dwarf Galaxy Survey detected at 500 μm showed the excess [56], when making use of the [62] models of dust emission. This implied that the effect is not common to all galaxies but becomes more pronounced in sources of lower metallicity. A large number of potential explanations were put forward (e.g., [47,56,63–66]):

- A particularly cold so far missed dust component.
- A long wavelength enhancement of the opacity of silicate grains.
- A kinetic temperature dependent grain emissivity, with the emissivity index $\beta_{\rm IR}$ decreasing when $T_{\rm kin}$ increases.
- Spinning grains.
- Cosmic microwave background (CMB) fluctuations.
- A positive correlation with the HI component.

- Blending with CO lines.

While a detailed discussion of all these suggestions is well beyond the scope of this paper, it is worth noting that the introduction of a so far missed very cold dust component would lead to very high $M_{\rm dust}/M_{gas}$ ratios, because at low temperatures dust emissivity per dust mass is very low. This cannot be reconciled with the fact that in metal poor galaxies $M_{\rm dust}/M_{\rm gas}$ values should be particularly low because dust grains require the inclusion of heavy elements (e.g., [47]). A similar argument also holds for CO (see Section 3.4).

Based on measurements of the Hβ line, a solution to this puzzle has been presented by [67]. After removing the stellar absorption component and accounting for extinction, the Hβ line permits the derivation of massive star formation rates, which also determines the flux densities of the free-free emission. This so-called bremsstrahlung can be significant in galaxies of low metallicity: because of high temperatures and low $M_{\rm dust}/M_{\rm gas}$ ratios, dust emission may start to dominate the continuum emission only at shorter wavelengths and higher frequencies than in larger more metal rich galaxies. Prior to [67] this was already mentioned by [68,69]. However, lacking accompanying Hβ data, they concluded that free-free emission should be insufficient to explain the submillimeter excess. The more metal poor a galaxy is, inhibiting a strong dust continuum at submillimeter wavelengths, and the more active the galaxy is with respect to star formation, enhancing the free-free emission, the more dominant bremsstrahlung becomes, creating a detectable 'excess' of continuum emission at wavelengths of $\gtrsim$500 µm (Figure 3; see also [70] and Section 5.2).

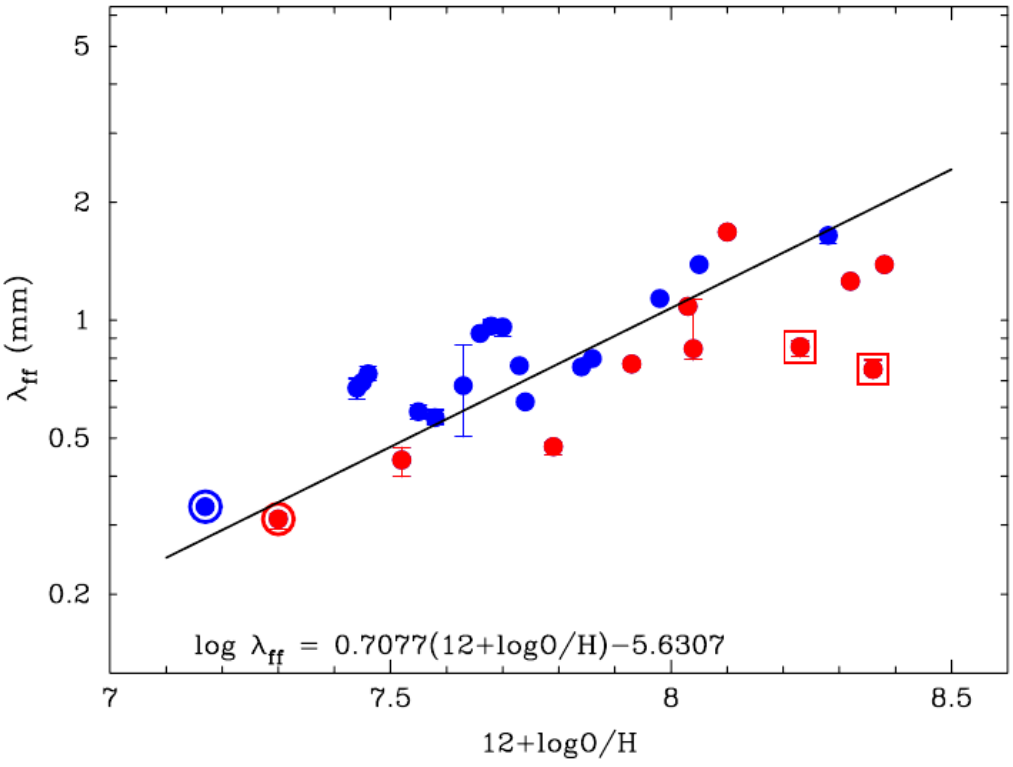

Figure 3. The wavelength at which dust and free-free continuum emission reach the same intensity level is plotted as a function of metallicity for galaxies with $L(\mathrm{H}\beta) < 10^7$ L$_\odot$ (blue filled circles) and $L(\mathrm{H}\beta) > 10^7$ L$_\odot$ (red filled circles). The correlation demonstrates how strongly metallicity affects the dust to free-free emission ratios, while the specific star formation activity of individual galaxies is leading to significant scatter. The encircled galaxies in the lower left are IZw 18 (blue) and SBS 0335–052 (red). The vigorously star forming galaxies Haro 11 and IIZw 40 are indicated by surrounding squares. The solid line is an unweighted fit to the shown *Herschel* sample with a total of 28 galaxies [67].

3.4. The Molecular Component

Showing (unlike H_2) a small but notable dipole moment, being heavy enough to reveal rotational transitions at mm- and submm-wavelengths and belonging to one of the most abundant species, CO is the most common tracer of molecular gas, in the Milky Way as well as in extragalactic objects. Thus it traces best the material being used for future star formation. The first CO map obtained from a dwarf galaxy, covering $2^\circ \times 2^\circ$ and published by [71] with a resolution of 8′.8, revealed the overall distribution of the molecular gas in the SMC. It indicated a low mass ratio (≈7%) of molecular (predominantly H_2) to atomic (predominantly HI) neutral gas and a high H_2 column density to integrated CO intensity conversion factor of $X(\mathrm{CO}) = N(\mathrm{H_2})/I(\mathrm{CO}) = 6 \times 10^{21}\,\mathrm{cm^{-2}\,K^{-1}\,km^{-1}\,s}$, ≈30 times the Galactic disk value ([72]). Nowadays, much higher sensitivities and angular resolutions can be achieved, basically confirming the trend suggested by this early paper (see below).

The lower the metallicity becomes, the more difficult it is to detect the molecular component of the gas. In galaxies with fractional oxygen abundances below that of the SMC ($12 + \log(\mathrm{O/H}) \approx 8.2$), very little CO is detected even in galaxies showing vigorous star formation (see, e.g., the patchy morphology of CO in NGC 6822 shown in Figure 4). The problem is that the shielding properties of CO are far weaker than those of H_2 because of much lower column densities. The lower the metallicity, the less carbon and oxygen are available to form CO and the lesser amounts of dust are available to shield these fragile molecules against the interstellar radiation field. When measured with single-dish beam sizes, i.e., with the *IRAM* 30 m, this leads to $\alpha(\mathrm{CO}) = M_{\mathrm{H2}}/L(\mathrm{CO}) \propto (Z/Z_\odot)^{-y}$ with $y \approx 3.3$ [48], ≈1.5 [73] or ≈2.0 [74]. As a consequence, there must exist large amounts of CO-dark molecular gas. Such gas is already known to cover significant volumes of molecular clouds in the solar neighborhood with its relatively high metallicity [75]. It should become even more predominant in dwarf galaxies with gas lacking carbon, oxygen and other metals. Therefore, in spite of often optically thick mm-wave CO lines, where a lower column density would not drastically change the peak line intensity, the volume of the region from where CO is emitted decreases and thus leads overall to reduced line intensities as long as the emitting region is not spatially resolved [72]. X(CO) and α(CO) thus also depend on the angular resolution [76,77].

To directly relate H_2 mass to CO column density independently of a conversion factor, the virial theorem can be applied to individual clouds as long as they are spatially resolved. However, its application should be viewed as an estimate of the mass confined to the CO emitting volume and not revealing this critical value for the entire molecular cloud or complex (e.g., [72]). A better way to quantify the total molecular gas mass is to combine several interstellar tracers (see Section 4.2).

As mentioned, CO observations become more and more difficult when the metallicity decreases. An interesting set of galaxies is that of [74], who detected CO in eight dwarf galaxies outside the Local Group that cover a metallicity range of $12 + \log(\mathrm{O/H}) = 7.7$–$8.4$. Nevertheless, the signal-to-noise ratio of the CO $J = 1 \rightarrow 0$ line of the lowest metallicity galaxy in this sample, CGCG 007–025, is with ≈3 quite low and indicates that at such a metallicity, ≲10% of the solar one, the *IRAM* 30 m is close to its sensitivity limit. For a similarly sized sample of BCDs (although at slightly higher metallicities) also studied with the *IRAM* 30 m, see [73].

To date, *ALMA*, the *Atacama Large Millimeter/submillimeter Array*, and *NOEMA*, the *Northern extended Millimeter Array*, provide by far the highest accessible sensitivity and angular resolution. A few exemplary dwarf galaxies have already been studied. The nearest one, still belonging to the Local Group, is NGC 6822 ($D \approx 474 \pm 13$ kpc; [78]). With a sub-SMC metallicity of $12 + \log(\mathrm{O/H}) = 8.02 \pm 0.05$, NGC 6822 has been observed in the CO $J = 2 \rightarrow 1$ transition [77] with an angular resolution of 0′.9, corresponding to unprecedented 2 pc (Figure 4) beyond the Magellanic Clouds. Observing four 250 pc sized areas that amount to about two thirds of the star formation activity in this galaxy reveal ≈150 compact CO clumps with sizes of only 2–3 pc and full half power line widths of $\approx 1\,\mathrm{km\,s^{-1}}$. The CO clumps only cover a tiny part of the observed area and there are

no such clumps in a fifth field outside the active zone of NGC 6822. Apparently, CO can only survive in tiny particularly well shielded pockets of interstellar gas. The clumps themselves follow with respect to size, column and spatial density and dynamics similarly sized clumps in the Milky Way. Only when considering larger linear scales does the low metallicity start to play a dominant role. An even more extreme object, the irregular galaxy Wolf-Lundmark-Melotte (WLM) with 12 + log(O/H) ≈ 7.8, studied by [79], revealed 10 isolated CO $J = 1 \rightarrow 0$ clumps with properties similar to those encountered in NGC 6822. One of the most extreme CO detected galaxies with respect to metallicity (12 + log(O/H) = 7.5; [80]), Sextans B (also known as DDO 70), has been mapped with *ALMA* by [81]. Using a linear resolution of 1.4 pc for this source located in the outskirts of the Local Group revealed five clumps, accounting for the bulk of the single-dish emission and following Larson's size-line width relation for the disk of the Milky Way.

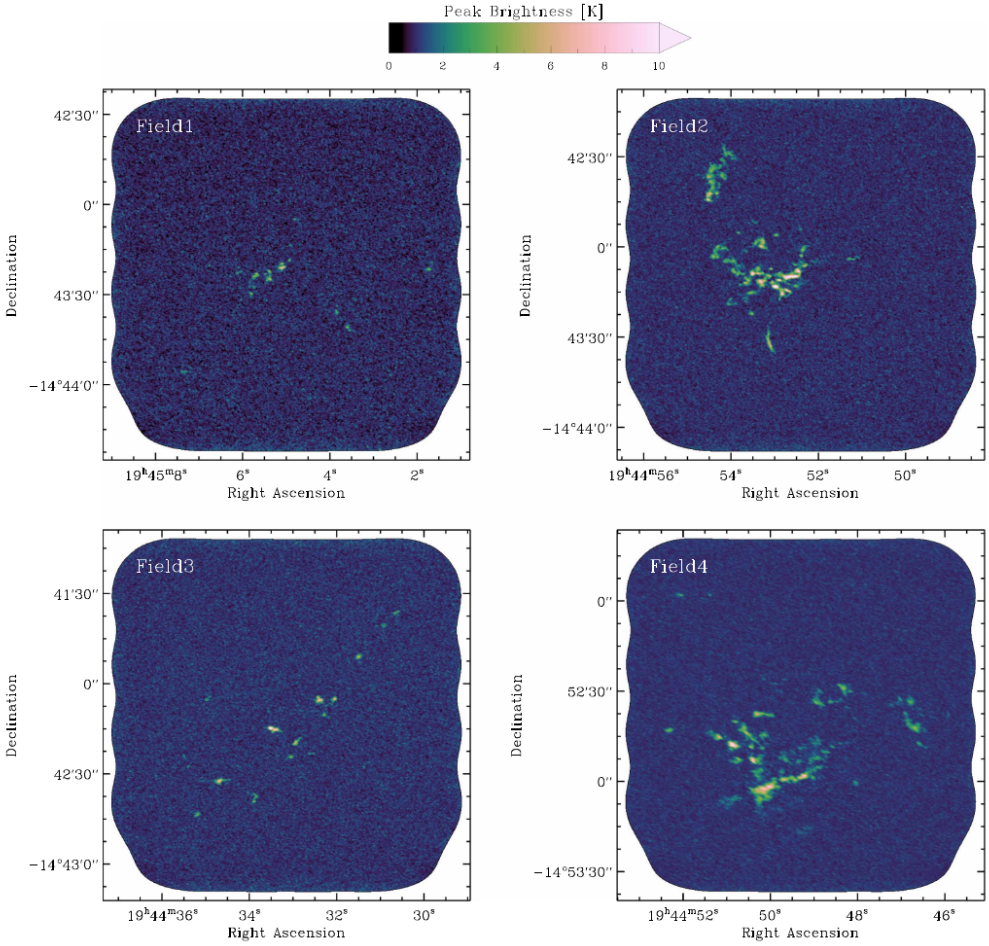

Figure 4. *ALMA* data with 2 pc linear resolution (0.″9) of four selected regions with star-forming activity inside of NGC 6822 taken from [77].

The prototypical BCD IIZw 40 with 12 + log(O/H) = 8.1 and $D \approx 10$ Mpc has been studied by [82], using *ALMA* in the CO $J = 1 \rightarrow 0$ to $3 \rightarrow 2$ lines. The system appears to have undergone a major merger. Beam sizes of 0.″5 correspond to linear resolutions of 24 pc, channel widths were 2 km s^{-1}. While there is a number of spatially unresolved CO clumps, the molecular emission is dominated by a central almost 100 pc sized elongated structure exhibiting line intensity ratios that favor the $J = 3 \rightarrow 2$ line and that are more reminiscent of Luminous InfraRed Galaxies (LIRGs) than normal star-forming objects. Possibly due to the interaction, the size-linewidth relation deviates from that in the disk of the Milky Way. Finally, Mrk 71, also known as NGC 2363 and located at a distance of 3.4 Mpc [83], contains two Super Star Clusters (SSCs). The clumpy CO condensations observed include

a component, exhibiting two velocity features, that coincide in projection with the SSC Mrk 71-A and may undergo momentum-driven feedback. For more information on SSCs, the present day counterparts of forming globular clusters, and their relation to a dense metal poor ISM, see the paragraphs on NGC 1140, SBS0335–052, and NGC 5253 in Section 5.2.

3.5. The Ionized Gas

Ionized gas is observed in various parts of the electromagnetic spectrum and can comprise, in dwarf galaxies, a significant fraction of the entire ISM mass (e.g., [84]). Starting with the lowest frequencies and longest wavelengths, ref. [85] revealed, after disentangling global thermal and non-thermal radio emission between ≈345 MHz and 24.6 GHz, that the synchrotron emission of most dwarf galaxies (the exception is IC 10) cannot be simulated with a single spectral index. While at lowest frequencies, an average spectral index of $\alpha = -0.59 \pm 0.20$ ($S_\nu \propto \nu^\alpha$; S: flux density) has been found, the synchrotron spectrum becomes steeper somewhere between 1 and 12 GHz, due to a break or an exponential decline (Figure 5). As a consequence, the free-free emission is stronger than previously anticipated, at least at GHz frequencies (see also Section 3.3). The non-thermal cutoff could be caused by the injection spectrum of cosmic ray electrons, and would then be consistent with the mean spectral index of supernova remnants [86].

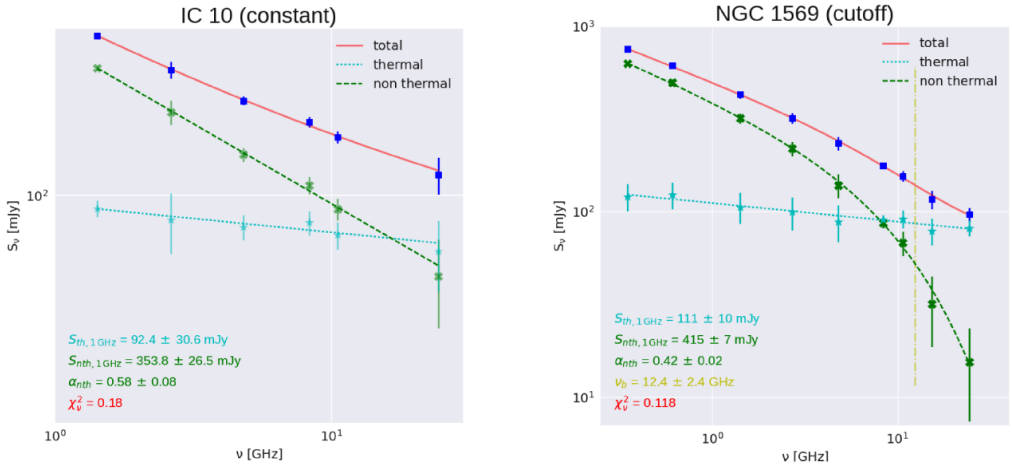

Figure 5. Global radio continuum spectra from IC 10 and NGC 1569, obtained by the Effelsberg 100 m telescope [85]. Measured flux densities: blue squares connected by a red solid line; free-free emission: cyan stars connected by a cyan dotted straight line; non-thermal emission: green crosses connected by a green dashed line. Characteristic parameters are plotted in the lower left, indicating the thermal and non-thermal contributions at 1 GHz. The vertical yellow dash-dotted line in the right panel denotes the break frequency (12.4 GHz), which is also given in the lower left of this panel. The nonthermal spectral indices at 1 GHz and the reduced χ^2 values of the fits are presented in the lower left corners of both panels.

Within the local volume ($D \lesssim 11$ Mpc) already discussed in Section 3.1 with respect to HI, Hα has been detected in 88% of the 379 late-type dwarfs, while the early-type dwarfs only show detections in 41% (50/122) of the targets [17]. Again this indicates that the late-type dwarfs tend to form stars more actively.

Finally, it is worth to mention the detection of [Ne V] in various dwarf galaxies, likely indicating fast shocks with speeds of several hundred km s^{-1}, even though the presence of a massive compact nucleus is another possible interpretation [87–89]. X-ray emission from BCDs is commonly dominated by binary stars, providing a component of intense hard radiation (e.g., [90]).

4. Star Formation and Active Nuclei

4.1. Star Formation

A major question is how stars are formed in small galaxies. The Milky Way shows continuous star formation including many active sites at a given epoch. And while the locations of these star-forming regions may change with time, their number and SFR, integrated over the entire giant body of the galaxy, remained approximately constant during the last few Gyr (e.g., [91,92]). Dwarfs appear to be different. The star formation history of Local Group dwarfs, shown by [28], involves spikes. While each galaxy has an individual star formation history, different from all the others, those galaxies with more recent star formation activity (which can be resolved in time much better than any such activity in the early days of the Universe) show brief periods of enhanced activity, clearly following the expectation of a bursty nature of star formation in small galaxies [93–95].

GALEX, the GALaxy Evolution eXplorer, was designed to observe the sky at ultraviolet (UV) wavelengths, 0.135 μm–0.28 μm. According to [17], 91% (430/474) of the late type dwarfs and almost all BCDs inside of D = 11 Mpc were detected by *GALEX*, while the corresponding number for early-type dwarfs is much lower (28%; 81/294). These values are consistent with the previously mentioned findings related to HI and Hα detection rates and emphasize the presence of a richer ISM related to massive star formation in the late-type sources. A comparison of far ultraviolet deduced star formation rates of late type dwarfs (T = 9–10) and spirals (T = 5–8) shows that present day star formation rates are compatible with the total stellar mass observed after 13.7 Gyr. This holds for both late type dwarfs and spirals. With M(HI)/M_* close to unity in late-type dwarfs (Section 3.1), it is not surprising that a similar correlation also holds when comparing for this type of galaxies the FUV deduced star formation rate not with the stellar but with the HI mass. The more crowded the environment, the larger is the scatter in sSFR = SFR/M_*, i.e., the specific star formation rate, because there are more galaxies that only show little star formation and are characterized by a low sSFR.

Star-formation rates from FUV luminosity refer to an equilibrium timescale of approximately 10^8 yr (e.g., [96]). SFRs from local dwarf galaxies (≈900 targets; $D < 11$ Mpc), based on FUV emission, exceed the average SFR over the age of the Universe by not more than an order of magnitude and reach this value only in exceptional cases [17]. sSFR values are not exceeding sSFR = $10^{-9.2}$ yr^{-1} versus an average of $10^{-10.1}$ yr^{-1} over a Hubble time. *Hubble Space Telescope (HST)* data of asymptotic giant branch and helium burning stars analyzed by [97] (23 targets) reveal highly individual star formation histories, like fingerprints, during the last 10^8 yr. For about half of them also a spatial progression of star formation is found (see [98] for a similar situation in dwarfs of the M 81 group). Major bursts beyond a factor of three over the average during the studied time interval (≈10^8 yr) are not encountered. This is in line with [96], who analyzed the Hα (characterizing a timescale of ≈5×10^6 yr) versus ultraviolet emission (timescale: ≈10^8 yr) of 185 local galaxies. Dwarfs near the upper end of our luminosity limit show burst amplitudes (with respect to their average SFR) not exceeding a factor of ten, while galaxies below $M = 10^{7.5}$ M$_\odot$ may undergo large and fast bursts, reaching an amplitude of up to two orders of magnitude over the average SFR, within a timescale of $t < 30$ Myr.

Hβ and UV luminosities should be considerably enhanced during the short periods of ongoing starbursts, with the Hβ emission decreasing more rapidly than the UV emission after the peak of the burst. This is because Hβ is emitted by younger and more massive stars. Therefore determining the UV and Hβ luminosities, both values can be extrapolated to a zero age, where the starburst was at its peak. Using these extrapolated peak values instead of the directly measured luminosities based on ≈14,000 compact star-forming galaxies at redshifts $z < 1$, ref. [4] succeeded in significantly reducing the scatter in the sSFR values, which is found to be independent of galactic stellar mass, further supporting the notion of a bursty mode of star formation in galaxies of small size, mass and luminosity.

During such a burst of star formation, observations suggest the presence of two modes: a more 'passive' and a more 'active' one. In the latter mode, the BCDs form SSCs, show high

column densities of H_2 and dust, including high dust temperatures. All this is confined to compact (<100 pc) regions. The less extreme mode shows instead more widespread and more diffuse gas with lower column densities [74,99]. Characteristic examples showing these two modes (e.g., SBS 0335–052 versus IZw 18; [84]) are discussed in some detail in Section 5.2.

4.2. Combining Different Interstellar Tracers

While we have already combined Hα or Hβ and UV emission to tackle the bursty nature of star formation in galaxies of low mass (see the last section), it is also noteworthy that at metallicities 12 + log(O/H) < 8.2, not only CO but also PAH emission becomes more and more elusive (e.g., [74,100]; Section 3.2). This is only indirectly related to metallicity and primarily due to a hard, intense radiation field [100]. Based on *ALMA* measurements of the Local Group dwarf NGC 6822 with a 2 pc linear resolution, ref. [77] finds that on pc-scales CO emission correlates well with PAH emission and less well with 24 μm emission. An anticorrelation is found with Hα. Thus PAH emission may be a possible alternative to CO as a tracer of molecular gas.

Using stacked averages of 1.4 GHz radio continuum and IR-70 μm Spitzer data, ref. [98] finds that the correlation between these two SFR tracers, observed in large galaxies on scales encompassing at least several 100 pc, also holds in dwarf galaxies. This may be the result of a 'conspiracy': the underabundance of dust due to low metallicities may be compensated by an easier escape of the cosmic ray electrons from supernovae, that give rise to the 1.4 GHz emission.

Characteristic HI distributions in actively star-forming dwarf galaxies show large (100–1500 pc) HI holes due to stellar feedback. With HI layers much thicker than in spiral galaxies (Section 2.2) gas densities are comparatively low, allowing for the formation of large shock-driven shells. While the smaller ones are filled with Hα emitting gas, the larger ones tend to show Hα along their rims (e.g., [101–104]). Typical expansion velocities are 5–10 km s^{-1}, not fast enough to release the gas into the intergalactic medium unless the galaxy has a mass well below 10^7 $M_\odot$ [105]. Hα and thermal X-ray emission may be correlated on global scales but not locally (e.g., [106]), with the hot gas possibly leaking out of the HII regions [107,108].

In regions of low metallicity, CO is able to trace the densest and most shielded cores inside of gas agglomerations mainly consisting of HI and H_2. However, it commonly only reveals a small fraction of the molecular environment. H_2 itself is also not providing a clear picture because it is homonuclear, lacking a permanent dipole moment. Due to its light weight, relevant frequencies are shifted away from radio wavelengths into the infrared and excited states are only found at levels >100 K above the ground state, too high to trace the bulk of the usually cooler molecular gas. Singly ionized carbon, i.e., the [CII] fine structure line at 158 μm, can help to complement CO and H_2 observations, even though it is an atomic constituent. [CII]λ158 μm is usually the strongest far-infrared line and thus, with respect to its intensity, a prominent coolant of the ISM. With the carbon ionization potential of 11.26 eV, well below that of hydrogen, 13.60 eV, singly ionized carbon is a multiphase tracer, including diffuse gas in the warm and cold neutral ISM, the warm ionized ISM and dense gas in photon dominated regions. While L([CII])/L(CO J = 1→0) ≈ 2000 in normal spiral galaxies and about twice as large in starburst environments of major galaxies, ratios tend to be much higher, up to 80,000, in dwarfs of low metallicity (e.g., [55]). This is accompanied by a milder increase in the [CI] to CO 1→0 ratio [109].

With [CII] potentially arising from ionized, neutral atomic and neutral molecular gas, the main question is how much these physically different environments can contribute to the observed strong line emission. This ambiguity constitutes the challenge of using this tracer to probe CO dark molecular gas. To give an example: Studying five positions in NGC 4214 (12 + log(O/H) ≈ 8.2) belonging to three separate regions with beam sizes of 12–14″ and using ancillary data from far infrared fine structure lines, HI and CO J = 1→0 and 2→1, ref. [110] finds that about 80% of the total molecular hydrogen mass is CO-

dark, i.e., not participating in CO emission. The method to quantify the contribution of the CO-dark molecular gas with respect to the entire molecular environment (e.g., [48]) may include a detailed comparison between the lineshapes of [CII] 158 μm, [NII] 122 μm and [NII] 205 μm, observable with *Herschel*, and HI and CO to kinematically discriminate between the various gas components. The observed features have then to be used to obtain estimates of column densities as a function of radial velocity. Assumptions on fractional abundances relative to hydrogen complete this process. In particular the latter steps related to the evaluation of column densities and fractional abundances lead to substantial uncertainties. Therefore, high quality data providing information on crucial parameters as a function of velocity are mandatory.

To summarize, L([CII])/L(CO $J = 1 \rightarrow 0$) luminosity ratios are largest in dwarf galaxies because the CO-dark gas is even more widespread there than in larger more metal-rich galaxies. The [CII] 158 μm line has become the main tracer of this CO-dark gas, although there may be exceptions (for one such exception, IZw 18, see [111]). The CO-dark gas apparently dominates the molecular environment of dwarf galaxies and [CII] can even be used to estimate X(CO) and α(CO) values ([112]; see also Section 3.4) and to test the Schmidt-Kennicutt star-formation law [113]. The latter relation connecting molecular and star-forming surface densities appears to be consistent with that of large galaxies [113,114], although the metallicity certainly plays a role in the fractional amount of the CO-dark mass. Nevertheless, the primary factor regulating this quantity is almost certainly the extinction characterizing the dense gas [48].

Finally, much effort has also been spent on chemical abundances, and the combination of tracers of different elements. Optical and near-infrared spectroscopy of HII regions allows for the detection of a plethora of lines from a number of abundant heavy elements that are not only constraining stellar evolution and the 'chemical' evolution of dwarf galaxies, but also the depletion of metals onto dust grains. While the latter effect is not as severe as in more metal-rich galaxies with higher dust-to-gas mass ratios (see also Section 2.2), the multitude of elements to be detected leads to a large number of notable correlations. To mention a few: [Mg/Ne] decreases with rising metallicity because Ne, unlike Mg, is a noble gas which is not significantly incorporated into dust grains. On the other hand, Mg and O depletion is less metallicity dependent than Fe depletion and data including SBS 0335–052, a galaxy with a particularly low metallicity close to 12 + log(O/H) = 7.0, indicate that C/O increases with O/H [32]. However, in view of the many elements involved, a detailed description of these relations is beyond the scope of this article. For details, see e.g., [32,58,115,116].

4.3. Active Galactic Nuclei and Outflows

Active galactic nuclei (AGN) have the potential to shape their parent galaxy and to severely affect its ISM. For a long time, searches for AGN in small galaxies of low mass were unsuccessful. Nevertheless, this is an important endeavour, because the study of central black hole candidates in dwarf galaxies would provide strong constraints to supermassive black hole (SMBH) seeds in the early Universe. In recent years, evidence for the presence of massive black holes is gradually growing. The low end of the black hole mass- velocity dispersion relation in Seyfert 1 and Seyfert 2 galaxies has been studied by [117–119]. The detection of AGN in five dwarf galaxies based on the presence of extraordinarily broad and luminous Hα lines has been suggested by [120,121]. The observed emission, with line widths in excess of 2000 km s^{-1} (see also [122]), could not be explained by supernovae, Wolf-Rayet stars or shocks propagating in circumstellar envelopes, either because these objects would not provide the observed high luminosities or because of a lack of variability over a time span of order 5 yr. An AGN is in this context the remaining, most likely explanation.

Employing adaptive optics from the *Gemini*/NIFS instrument complemented by *HST* imaging, ref. [123] reported the likely discovery of supermassive nuclear engines ($M > 10^6$ M$_\odot$) in two ultracompact dwarf (UCD) galaxies of the Virgo cluster. This is consistent with the idea that such objects represent stripped nuclear regions of previously

more extended galaxies. Based on the discovery of a hard X-ray source at the dynamical center of Henize 2–10, [124,125] reported the presence of an accreting black hole in this galaxy, surrounded by forming super star clusters. Following [126], the mass of the nuclear object is $\approx 3 \times 10^6\,M_\odot$, the uncertainty being a factor of a few. Nevertheless, the absolute magnitude of this galaxy is with $M_V \approx -19^M$ slightly above the luminosity limit we defined for dwarfs in Section 1. Another candidate galaxy, with similar visual luminosity, is NGC 5408, where [127] suggested the presence of a nuclear source based on X-ray, optical and radio observations. While the X-ray emission from these sources could serve as a model, ref. [128] did not detect strong hard UV or X-ray emission from the putative accretion disks around candidate black holes in small galaxies that show particularly strong and wide emission lines of ionized gas.

Using the Baldwin-Phillips-Terlevich BPT diagram [129] and connecting [OIII]/Hβ with [NII]/Hα line intensity ratios, ref. [130] identified among ≈2500 SDSS targets 136 dwarf galaxies with line ratios indicating the presence of an AGN. A small fraction of these sources also shows broad Hα emission. Using the virial theorem, the median mass of the putative AGN is estimated to be $M = 2 \times 10^5\,M_\odot$. It should again be noted, however, that the median absolute magnitude of these objects is $M_g \approx -18^M$, so that a significant fraction of these galaxies is more massive than the true dwarfs discussed in this article (Section 1). Addressing galaxies with lower masses more consistent with our definition of dwarfs, ref. [131] detected [Fe X]λ6374 coronal line emission in 81 galaxies with $M_* < 3 \times 10^9\,M_\odot$. This emission is found to be too strong to be emitted by stellar sources and even supernovae are not able to explain the majority of the observed lines.

To summarize, the systematic study of massive black holes in dwarf galaxies has just begun. It will be interesting to see the impact of these studies on our understanding of formation of and feedback from massive nuclear sources in the early days of the Universe [131–140].

5. Star Forming Dwarfs in the Local Universe

5.1. Are There Young Dwarfs in the Local Universe?

Analyzing ≈280,000 and 400,000 SDSS spectra, ref. [141,142] searched for galaxies that may have formed most ($\gtrsim$50%) of their stellar component during the last Gyr, while lacking an active galactic nucleus. Because of a lower mass cutoff at $M = 10^8\,M_\odot$, metallicities (12 + log(O/H) = 7.9–8.6) are at the upper end of what is being considered here (Section 1). When compared with a control sample involving the same selection criteria but requiring a predominantly older stellar population, the potentially young galaxies are bluer, have higher sSFRs and surface brightnesses, and are relatively dusty, compact, asymmetric and clumpy. Furthermore, they are with respect to HI significantly more gas rich and tend to reside in the inner parts of low-mass groups. Appearing to be relatively frequently affected by interactions, they may have been activated by such an event. Modelling galaxy formation and trying to simulate the number of such young galaxies in the local Universe, ref. [143] provides predictions for a wide range of scenarios. These, including or excluding dark matter, yield results that differ by several orders of magnitude, emphasizing that the systematic observation of young local galaxies could become an important constraint to galaxy formation and the evolution of the Universe.

There are galaxies with particularly low gaseous metallicities, reaching 12 + log(O/H) = 7.0 in the local volume ($z < 1.0$) [144–147]. These galaxies may be affected by particularly inefficient star formation and/or severe losses of metal enriched matter due to supernovae or large scale galactic winds. These galaxies also contain a predominantly young stellar population. Investigating large samples of galaxies from the SDSS, the minimal metallicities encountered in these galaxies provide, like the above mentioned number of potentially young galaxies, important clues for the formation and evolution of galaxies during the last 13 billion years.

Finally, it is worth mentioning a substantial lack of almost purely gaseous agglomerations on galaxy scales in the local Universe. An area of 36 deg^2 was surveyed in HI with the 64 m *Parkes* multi-beam system [6], with 129 sources detected. The same area

was also observed with the *UK Schmidt Telescope* reaching a limiting surface brightness of $\mu_R = 26\overset{m}{.}5\,\mathrm{arcsec}^{-2}$; no optically dark HI galaxies were found. Such galaxies must either be rare, gas poor or otherwise outside their detection limits.

5.2. Some Outstanding Targets

In the following we discuss properties of local individual sources that illustrate the large variety of metal-poor actively star forming dwarf galaxies, on the basis of what has been described in previous sections. This will be complemented, in Section 6, by dwarf galaxies at cosmologically relevant distances. The chosen order of the sources in the following subsection does not reflect physical properties but merely the right ascension of the targets.

IC 10 (UGC 192): IC 10 is commonly classified as a Local Group dwarf iregular at a distance of ≈800 kpc with $M_B = -16\overset{M}{.}7$ and an oxygen abundance about 1/4 solar (e.g., [148]). It is, like NGC 4449, one of those few galaxies with an HI envelope that extends far beyond its optical diameter, encompassing an angular size of a full degree [149–153]. The velocity gradient along the major axis is opposite to that in the core of the galaxy, possibly indicating a non-planar highly warped HI disk, again similar to that seen in NGC 4449. There are holes in the HI distribution, likely a consequence of supernovae or stellar winds [154]. Modeling the ionized gas through observations of mid- and far-infrared fine structure lines and the photoionizaton code CLOUDY, ref. [155] finds that most ionized clumps, irrespective of their size, show hydrogen densities of order $10^{2.0}$ to $10^{2.6}\,\mathrm{cm}^{-3}$ and ages of about 5 Myr. The larger sized clumps are more radiation bounded than the smaller ones, while [CII], [SiII] and [FeII] emission mostly originates from the neutral gas.

Most of the star-forming activity of this galaxy inside the Local Group is taking place in an elongated $3' \times 1'.5$ sized region extending from the northwest to the southeast, as seen in 2MASS 2 μm emission [148] and in the ≈10 GHz radio continuum [156]. Two 22 GHz H_2O masers are found in this region [157,158], indicating ongoing vigorous star formation. This is complemented by the presence of massive molecular clouds traced by CO [157,159,160]. The emission includes 14 Giant Molecular Clouds (GMCs) with sizes, CO luminosities, line widths and X(CO) conversion factors similar to the values found in the Galactic disk. The star-forming rate per molecular mass is higher than in most other galaxies, confirming that IC 10 is presently undergoing a starburst.

NGC 147 (UGC 326), NGC 185 (UGC 396) and NGC 205 (UGC 426): The three dwarf ellipticals with absolute visual magnitudes of $M_V = -15\overset{M}{.}0$, $-15\overset{M}{.}0$ and $-16\overset{M}{.}2$ (NED[2]), respectively, are companions of the Andromeda galaxy and are therefore nearby, offering the possibility to study their ISM in spatial detail. In line with the highly individual star formation histories of Local Group dwarfs already mentioned in Section 4.1, they offer a useful insight into the variety of properties one may encounter when analyzing galaxies that appear to be similar at first sight. This holds in particular for NGC 147 and NGC 185: Luminosity, mass, metallicity, and size are extremely similar. However, NGC 147 does not possess a significant ISM, while NGC 185 does, and also contains a young stellar component (e.g., [32]). NGC 205 does not only host an ISM and a young stellar component, it is also nucleated, with a stellar cluster at its core (e.g., [161]). Its neutral atomic and molecular ISM, comprising within a factor of a few $M \approx 10^7\,M_\odot$ [145], shows similar morphologies and kinematics on 90 pc scales [162,163]. There are attempts to reveal a massive nuclear engine at its center (e.g., [164,165]). So far, based on stellar dynamics, a value of $M_{BH} \sim 7 \times 10^3\,M_\odot$ has been proposed by these authors, both as a 3σ upper limit and as an actual value. However, in view of systematic errors and the possibility of a cluster of dark stellar remnants, this can only be considered as tentative.

SBS 0335–052 and IZw 18 (Mrk 116): The first target consists of a pair of two BCDs, SBS 0335–052W and SBS 0335–052E (see Figures 6 and 7), embedded in a common HI cloud [166,167] and exhibiting vigorous star formation. This includes the presence of young SSCs, possibly a consequence of their interaction. The most interesting aspect of this system ($D \approx 55$ Mpc; $M_V \approx -16\overset{M}{.}8$, [168]) is its extremely low metallicity. For the brighter

eastern source [60] find 12 + log(O/H) = 7.11–7.32 in different HII regions. In the fainter, western one projected 22 kpc away from SBS 0335–052E they obtain for the main source 12 + log(O/H) = 7.22 ± 0.07. However, in three less conspicuous ionized bubbles, the metallicity is exceedingly low, with values of 7.01 ± 0.07, 6.98 ± 0.06 and 6.86 ± 0.14. Thus SBS 0335–052 is a clear candidate for the class of 'young dwarfs' discussed in Section 5.1. The spectral energy distribution (SED) of SBS 0335–052E (see Figure 8) covering six orders of magnitude in wavelength shows the typical peaks due to stellar emission near optical wavelengths and the dust emission in the infrared, as well as additional free-free emission at longer wavelengths [51]. Noteworthy is that even at 870 μm (≈345 GHz) almost 90% of the emission appears to represent free-free emission, likely because the ISM is affected by (1) a high level of star formation and (2) a low dust-to-gas mass ratio (see also Section 3.3). CO remains undetected [169].

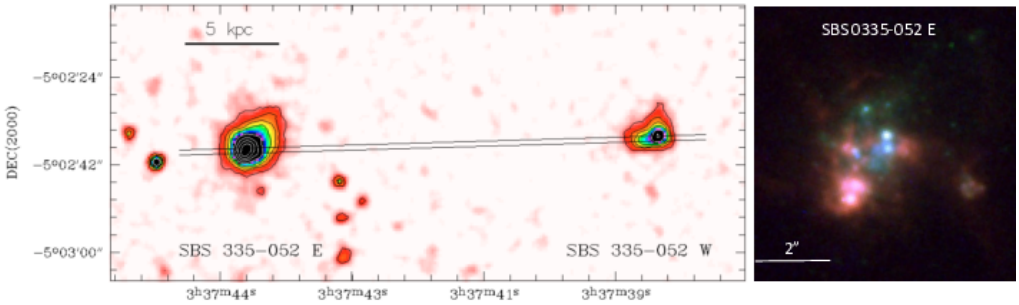

Figure 6. Left: A B-band image taken from the *Calar Alto* observatory showing the western and eastern components of SBS 0335–052. The black lines indicate the location of a slit used for optical and near infrared spectroscopy. Taken from [60]. **Right**: A composite true-color HST/ACS image of SBS 0335–052 that illustrates the super star clusters in the eastern source. Taken from [170].

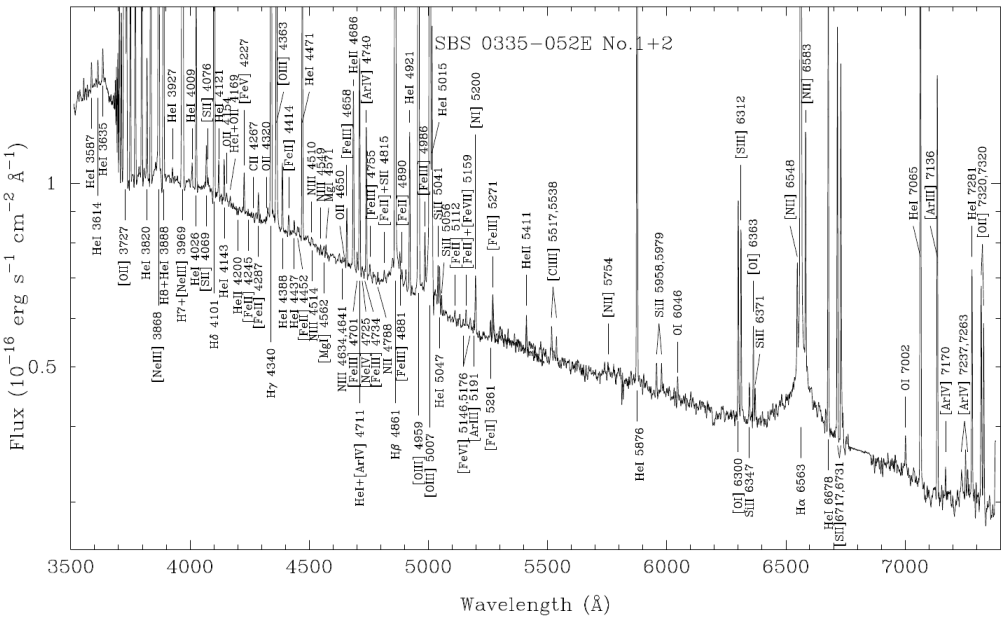

Figure 7. A FORS high-resolution spectrum taken with the *Very Large Telescope (VLT)* of the European Southern Observatory (ESO) from the two southern SSCs of SBS 0335-0052 (see Figure 6, right panel), employed to derive metallicities. The spectrum, showing particularly wide hydrogen recombination lines, was published by [60].

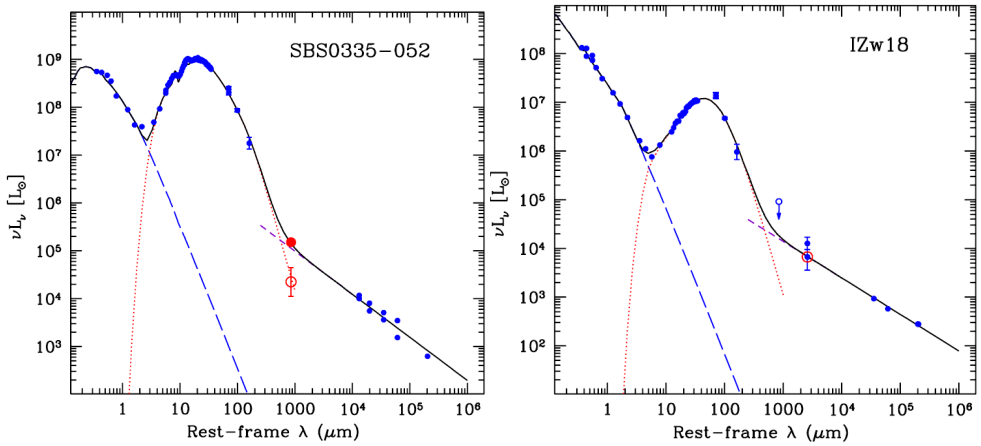

Figure 8. Spectral Energy Distributions (SEDs) from SBS 0335–052 (**left**) and IZw 18 (**right**). The black lines respresent fits using DUSTY models, the blue dashed lines show the stellar contributions, the dotted red lines give the contributions from the dust and the dashed purple straight line (mostly undistinguishable from the total emission) provides the radio continuum at long wavelengths. **Left**: The filled red circle indicates the total λ = 850 μm continuum emission from $0\farcs7 \times 0\farcs45$ *ALMA* data, while the empty red circle stands for the dust contribution. **Right**: The empty red circle surrounds the dust contribution suggested by [171], while the blue filled circle above includes the entire λ = 2.6 mm emission. From [51].

Following the definition in Section 5.1, IZw 18 might be another young galaxy, although this is matter of debate because of the presence of evolved stars [172,173]. It also hosts HII regions of extremely low metallicity, 12 + log(O/H) = 7.17 ± 0.03 in the northwestern and 7.18 ± 0.03 in the southeastern component [174]. Showing extremely weak CO emission [175], the galaxy may still be in the process of formation [176]. IZw 18 is with $D \approx 18$ Mpc ($M_V \approx -15\fm0$; NED) much closer to us than SBS 0335–052. No red giant is found in measurements 1–2 magnitudes deeper than the expected tip of the red giant branch. Many stars appear to be younger than half a billion years, a time during which up to three bursts of star -formation can be deduced, interrupted by more quiescent periods lasting 1–2 $\times$ 10^8 yr. Far UV (917–1188 Å) absorption lines [177] do not indicate the existence of dominant galaxy-wide in- or outflows. Based on *HST* far UV absorption line data, ref. [50] investigated the metallicity of the massive HI envelope of IZw 18. It is as in SBS 0355–052 [167] not zero, but roughly two thirds of that derived from the HII regions. They argue that at least a part of this metallicity must have been generated prior to the present starburst, suggesting the existence of an older stellar generation.

Comparing SBS 0335–052 with IZw 18, these two systems with extremely low metallicities may be good examples of the two starburst modes in dwarfs suggested earlier at the end of Section 4.1. SBS 0335–052 would then represent the 'active' and IZw 18 the 'passive' mode. The infrared luminosity of SBS 0335–052 is with $\approx$1.6 $\times$ 10^9 $L_\odot$ versus $\approx$2 $\times$ 10^7 $L_\odot$ for IZw 18 almost two orders of magnitude higher, indicating quite different levels of star-formation activity [51]. At radio wavelengths, the two galaxies show very different spectra: while IZw 18 has a relatively straight power-law indicative of optically thin thermal emission combined with synchrotron radiation, SBS 0335–052 is self-absorbed (e.g., [178–180]). This indicates ionized gas densities of 3000 to 5000 cm^{-3}, much higher than the implied densities of $<$100 cm^{-3} in IZw 18 [181]. Another major difference between the two galaxies is the peak position of their IR-dust SEDs. Both show maxima at short wavelengths, compatible with the relatively high dust temperatures characterizing dwarf galaxies (Section 3.2). However, while IZw 18 peaks at 50–60 μm, SBS 0335–052 is truly extreme showing its maximum in the range 20–30 μm (Figure 8), thus indicating a lack of a cool dust component. In view of these differences we conclude that metallicity is not the only factor that shapes dwarf galaxies with an extremely unprocessed interstellar medium.

NGC 1140 (Mrk 1063): NGC 1140 (Figure 9) is a barred irregular galaxy at a distance of ≈20 Mpc with a metallicity of about 12 + log(O/H) = 8.2 [74]. Its irregular morphology, revealed by Hα images [182] shows a southwestern chain of HII regions, the tail, and a northern region, the head, which dominates the emission and star forming activity. This head, with 30 times the Hα luminosity of the giant HII region 30 Dor in the LMC [183], is surrounded by less conspicuous star forming regions. The dominant complex, about 500 pc in size, contains 6–7 blue SSCs [183,184], the most luminous of them consisting of several thousand O stars [185]. There is no galactic scale outflow, but violent shocks from the SSCs are disrupting the ISM on scales of 1–2 pc [182]. Shape and activity of the galaxy may be caused by a merger [182,183].

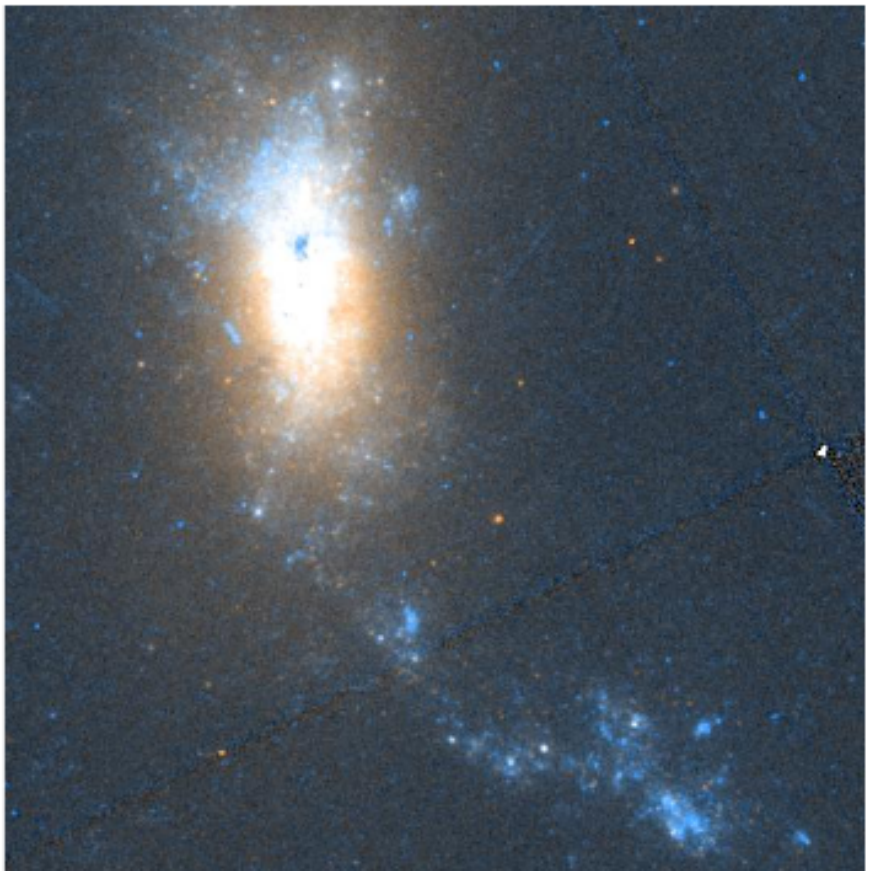

Figure 9. A composite *HST* image of NGC 1140, taken from [74].

As in NGC 5253 (see below), CO is highly excited and not optically thick, with $J = 3 \rightarrow 2$ line flux densities far surpassing those of the $J = 1 \rightarrow 0$ line. Naively, one would therefore expect high kinetic temperatures of the molecular gas giving rise to the observed CO emission. However, model fits including the dust continuum and molecular and atomic abundances relative to hydrogen [109] reveal high densities ($n(H_2) > 10^5$ cm^{-3}) but low temperatures ($T_{kin} \approx 20$ K), CO/CI ≈ 0.1, ^{12}CO/^{13}CO $\approx$ 8–20 and N(CO) $\approx 5 \times 10^{16}$ cm^{-2} for a realistic gas-to-dust mass ratio of ≈380 [109]. The low kinetic temperature in combination with a rather low opacity ($\tau(J = 3 \rightarrow 2) \approx 0.2$) can be explained if we assume that CO is only existing in spatially highly confined particularly well shielded pockets, where irradiation by UV photons is not as strong as elsewhere in the complex. Overall, the CO fractional abundance turns out to be $\approx 8 \times 10^{-7}$, two orders of magnitude below the commonly encountered value (HCN remains undetected). This is similar to the situation in the massive star forming region N159W of the LMC, where ammonia (NH_3), overall also highly underabundant, provides a temperature of only ≈16 K [186], while H_2CO, a molecule which is less sensitive to ionizing radiation, shows kinetic temperatures of order

50 K [187,188]. Presumably, there is no chance to detect NH_3 in NGC 1140. Here CO plays the role NH_3 is playing in the LMC because of its sensitivity to the strong ionizing radiation fields at low metallicity.

The extremely low $^{12}CO/^{13}CO$ abundance ratio obtained by [109] is smaller than any value encountered in the ISM of the Milky Way (see [189] for an analysis of the region with the lowest Galactic values, the Central Molecular Zone (CMZ) of the Galaxy). It does not reflect the real $^{12}C/^{13}C$ isotope ratio but must be caused by fractionation, i.e., by chemical charge exchange reactions that can reduce the $^{12}CO/^{13}CO$ abundance ratios to values below 20 (Figure 10), even if the actual $^{12}C/^{13}C$ isotope ratio is similar to that in the LMC, i.e., of the order of 55.

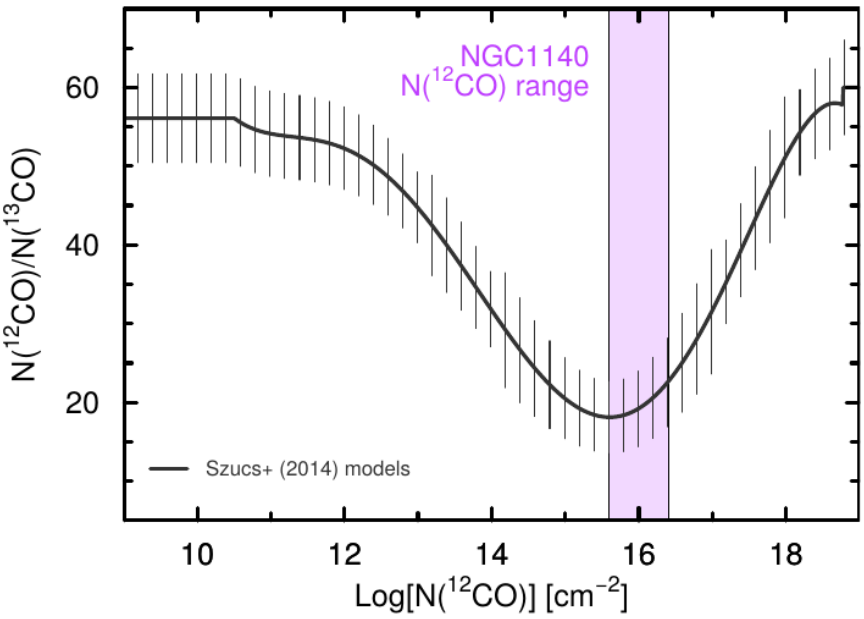

Figure 10. The carbon isotope ratio $^{12}C/^{13}C$ as traced by CO is plotted against the CO column density. The degree of fractionation follows the models of [190]; taken from [109].

NGC 5253: At a distance of about 4 Mpc and with a metallicity of the order of 12 + log(O/H) = 8.25 [191,192], the BCD NGC 5253 is one of the best examples to study the birth and evolution of SSCs as well as the interaction between densely packed massive stars and the surrounding gas. Not unexpected in view of the SMC-like metallicity of NGC 5253 (see Section 3.4) the *ALMA* data from [192], obtained with an angular resolution of $0\farcs2$ (≈3 pc), reveal 118 individual CO clumps. The most prominent object associated with a nascent SSC is a cloud termed 'D1', which contains within a diameter of only about 6 pc around 1500–2000 O stars [193]. Therefore it represents a promising candidate for the existence of a top heavy initial mass function (IMF). The correlation between CO line width and cloud size provides enhanced line widths by 0.2–0.3 dex with respect to Galactic disk clouds in the most active regions. The ionized gas comprises (as in Mrk 71, see Section 3.5 two components that are offset in velocity and in this case also in position [194]. These *JVLA* observations at an angular resolution of $0\farcs15$ also show an arm of ionized gas reaching out of the center in northwestern direction, possibly indicating feedback.

To further focus on D1, the most extreme source in the galaxy: the age of its SSC is estimated to be only $\approx 10^6$ yr, far too young for any supernova event [195]. The numerous massive stars must create isolated bubbles of ionized gas. However, surprisingly, the effect of the ionizing radiation and the stellar winds of the numerous massive stars leave the parent CO cloud mainly undisturbed. Mass loading by a large number of associated lower mass stars downstream of the flows could enhance the cooling and confine the hot shocked winds from the massive stars [196]. Nevertheless, these hot shocked winds have to merge in the future, then providing a large scale galactic wind.

6. Star Forming Dwarfs in the Cosmological Persepctive

6.1. Primordial Abundances

Dwarf galaxies contain matter that is relatively unaffected by contamination from stellar ejecta. Therefore they are suitable targets to trace the abundances of those nuclei that are, according to the standard model, products of Big Bang nucleosynthesis. These nuclei are deuterium (D), the stable rare isotope of helium (^{3}He), the main helium species (^{4}He), and the most common lithium isotope (^{7}Li). Abundances can be studied taking spectra of nearby objects with low metallicity. The two keystones to constrain Big Bang nucleosynthesis are deuterium and the main helium isotope. The former is most conveniently determined in damped Ly-α absorption systems towards quasars at high redshift, which is outside the scope of this article, while ^{4}He is to date most accurately traced by sensitive observations of HII regions in local metal poor dwarf galaxies (e.g., [197–204]). In such environments it is acceptable to assume that there is a linear correlation between helium and oxygen abundances, so that an extrapolation to an oxygen abundance of zero, the primordial value, can be carried out. Nitrogen or sulfur abundances may also provide a useful anchor. With respect to oxygen, it is important to include the weak [OIII]λ4363Å line, which requires regions of high electron temperature, potentially leading to a notable effect due to collisional excitation. To unravel the physical conditions of the gas, the inclusion of the He I line at λ = 10830 Å [197] adds essential information, thus reducing errors in the helium abundance considerably. Combining the results of the above mentioned eight articles results in a helium abundance by mass of Y_p = 0.2462 $\pm$ 0.0013 relative to hydrogen. Weighting the values with the inverse square of the given errors yields instead Y_p = 0.2475 $\pm$ 0.0015, the uncertainty representing again the error of the mean. This is in line with the helium abundance deduced by the *Planck* satellite determination of the baryon density, Y_p = 0.2471 $\pm$ 0.0003 (e.g., [203]), being consistent with three kinds of neutrinos and a lifetime for free neutrons of the order of 870 s.

6.2. Dwarf Galaxies Near and Far

Beyond helium abundances, compact local galaxies experiencing vigorous star formation are cosmologically relevant also in another important aspect: They may be similar in many respects to those of compact, also vigorously star-forming galaxies in the early Universe. Samples of such local low metallicity dwarfs with luminosities greatly affected by young stars have been collected (e.g., [205–207]). A detailed comparison of compact galaxies at low redshift as analogues of high redshift star-forming galaxies has been carried out by [208]. 25,000 compact star-forming $z < 1.0$ galaxies from the Sloan Digital Sky Survey (SDSS) have been selected and their properties were compared with those of galaxies at $z > 1.5$, deduced by various authors (e.g., [209–212]). Those low redshift galaxies with Hβ equivalent widths $\gtrsim$100 Å and being located in the star-forming region of the BPT diagram (Baldwin et al., 1981) show remarkable similarities with their higher redshift cousins. This concerns fractional oxygen abundances (12 + log(O/H)), stellar masses (M_*), far UV absolute magnitudes (M_{UV}), star formation rates (SFR), specific star-forming rates (sSFR), UV continuum slopes (β_{UV}), [OIII]λ5007/[OII]λ3727, [NeIII]λ3868/[OII]λ3727 and [O/Fe] ratios as well as [OII]λ3727, [OIII]λ5007, and Hα equivalent widths. As a consequence, the nearby galaxies can be taken as useful proxies for their more distant counterparts. In addition, the nearby galaxies can be traced to absolute magnitudes and linear resolutions that are not yet accessible at high redshifts. Thus they provide information that can be used to guide future observations as for example sensitive deep field measurements that may be obtained with the *James Webb Space Telescope* (*JWST*) covering galaxies in the early Universe (e.g., [213]).

6.3. The Role of Dwarfs at Reionization

Quasars are known to inject copious amounts of Lyman continuum (LyC) photons into the intergalactic medium (IGM), contributing to the reionization of the Universe. However, at redshifts z = 6–10, QSOs are rare and thus not numerous enough to drastically change

their large scale environment alone. While binary stars and less active galactic nuclei may provide additional energetic photons, models indicate that the participation of a multitude of small low-mass, low-metallicity systems may predominantly contribute the required LyC photons for the rapid reionization of the IGM (e.g., [213–215]). So far this galaxy population, characterized by low absolute magnitudes and luminosities, is below the detection threshold of even the most sensitive telescopes at the required redshifts (e.g., [5]). Furthermore, it is difficult to assess the Lyman continuum at the relevant redshifts because of attenuation by the still mostly neutral IGM and interlopers at $z < 6$.

Therefore, by observing $z > 6$ galaxies, it is not possible to establish a relationship between the leakage of LyC photons into the IGM and the detailed properties of these galaxies. This can only be revealed by observations of galaxies at lower redshift and numerous studies have been published to achieve this goal (e.g., [216–222]). Several ways have been suggested to find galaxies with high LyC leakages. Galaxies with a deficit of emission of optical lines representing a low degree of ionization, e.g., [SII], can be used in this sense. Other tracers are strong Lyα emission or high [OIII]λ5007/[OII]λ3727 line ratios (see [223] for a particularly extreme galaxy in the latter sense). However, these correlations show a significant amount of scatter. The He I λ3889 Å line in connection with Hβ, the [CIII]λ1909 transition, the Mg II 2796/2803 Å doublet and the UV HI Lyman series were also reported to be suitable tracers to gain insight into the opacity of the sources and their ability to allow LyC photons to escape [224–228].

Obtaining with the *HST* the near-IR SEDs (in the framework of observed wavelengths) from a large number of individual stars, estimating their ionizing flux and comparing these fluxes with the amount absorbed by dust and by ionizing the surrounding medium, escape fractions of several 10% were obtained for the nearby dwarf galaxy NGC 4214 [229]. Another promising way to identify LyC leakers appears to be the analysis of Lyα line profiles (e.g., [218,219,230]). Lyα lines peaking slightly off the systemic velocity and, even better, double peaked profiles separated by $\lesssim$300 km s^{-1} and down to $\approx$150 km s^{-1} around the systemic velocity in the most suitable cases are indicators of significant LyC leaking fractions. The double peaked lines are due to resonance scattering effects with small velocity spacings indicating low column densities (e.g., [231]). At high redshifts, the blue peak should be absorbed by neutral foreground gas due to the Hubble expansion, unless the source possesses a high peculiar motion away from us and/or a large ionized bubble surrounding it. More locally, due to the widespread ionized IGM, this is clearly a lesser problem. Interestingly. a first potential LyC leaker from the reionization epoch, at redshift z = 6.593, may have been directly observed by [232], suggesting the presence of an extended ionized bubble even at such a high redshift.

Analyzing the past of the ultra-faint galaxy (UFD) population of the Local Group, the small volume where such galaxies can be detected with highest sensitivity, ref. [233] suggests that the ancestors of such UFDs produced a significant amount (10–50%) of the UV flux required to reionize the IGM. Therefore the Lyα leakage of such or slightly larger galaxies is an essential parameter when considering the evolution of the Universe during those early days. This implies that more detailed measurements of the Lyα leakage of nearby metal-poor dwarfs are essential to observationally constrain the models and to create a more realistic picture of the time a few hundred million years after the Big Bang.

7. Future Prospects

Studies of the interstellar medium of dwarf galaxies are presently undergoing a major revolution. Using focal plane array technology, Apertif (APERture Tile in Focus) in the Netherlands, ASKAP (Australian SKA Pathfinder) in Australia and MeerKAT in South Africa are designed to cover simultaneously vast areas of the sky. The latter two of these facilities are also pathfinders for the Square Kilometer Array (SKA), which will provide yet another step ahead in sensitivity and angular resolution with respect to low frequency radio waves, covering the $\lambda \approx 21$ cm line of HI and the radio continuum. Furthermore, at optical wavelengths and in the near and mid infrared, the *James Webb Space Telescope* (*JWST*)

may provide observations with unprecedented quality in the range 0.5 μm–28 μm. Finally, with the new generation of large telescopes for optical, near infrared and UV mesurements (e.g., the *Extremely Large Telescope* (*ELT*)) it will be possible to determine $L_{\rm UV}$ and $L(\rm H\alpha)$ of high redshift galaxies, thus studying star formation histories in dwarfs outside the local volume.

With respect to the interstellar medium of dwarf galaxies, many questions are still not settled. What is for example triggering the enhanced activity of BCDs and, even more so, the Green Peas? Can the tentatively deduced presence of massive but presumably not supermassive ($M < 10^6\,\rm M_\odot$) nuclear engines be verified? What is their number and what are the properties of their parent galaxies with respect to other relevant physical paremeters? Will this shed light onto black hole seeds in the distant early Universe? And what will become the most convincing tool to detect such nuclei: The Lyα line shape, coronal lines or yet another tracer? How frequent are galaxies consisting almost entirely of neutral hydrogen gas as a function of redshift? Are they much more common at higher redshifts than locally? And is there evidence for high-J CO lines in clouds with nascent super star clusters complemented by hot dust and perhaps even by an X-ray dominated region (XDR) caused by the X-ray emission of the numerous newly formed massive stars? These and many other questions, some of them addressed in the accompanying articles, will keep dwarf galaxies in the focus of contemporary astrophyical research and will continue to attract a high degree of interest in these seemingly inconspicious but very numerous galaxies, that provide a great amount of information on the evolution of the Universe, at present times, in the distant past and as a consequence also on its future.

Author Contributions: Mostly written by C.H., L.K.H. and Y.I.I. provided essential contributions by (1) correcting the text, (2) providing a substantial number of papers that would otherwise have been overlooked, (3) suggesting relevant topics (e.g., the work of Klein et al. 2018 on the radio continuum) and (4) explaining complex scientific issues related to those papers, in which they were directly involved. All authors have read and agreed to the published version of the manuscript.

Funding: This research received no external funding.

Institutional Review Board Statement: Not applicable.

Informed Consent Statement: Not applicable.

Data Availability Statement: Not applicable.

Acknowledgments: We appreciate the very positive and constructive comments of the anonymous referees. Y.I.I. acknowledges support from the National Academy of Sciences of Ukraine (Project 0121U109612: 'Dynamics of particles and collective excitations in high energy physics, astrophsyics and quantum microsystems'). The article made use of the Astrophysics Data System and the NASA/IPAC Extragalactic Database.

Conflicts of Interest: The authors declare no conflict of interest.

Notes

[1] e.g., ned.ipac.caltech.edu/level5/Sept02/Palco-BCD/Agpaz3.html.

[2] NASA/IPAC extragalactic database, ned.ipac.caltech.edu.

References

1. Schechter, P.L. An analytic expression for the luminosity function for galaxies. *Astrophys. J.* **1976**, *203*, 297–306. [CrossRef]
2. Marzke, R.O.; Da Costa, L.N. The galaxy luminosity function at $z \leq 0.05$: Dependence on color. *Astron. J.* **1997**, *113*, 185–196. [CrossRef]
3. Ellis, R.S. Faint blue galaxies. *Annu. Rev. Astron. Astrophys.* **1997**, *35*, 389–443. [CrossRef]
4. Izotov, Y.I.; Guseva, N.G.; Fricke, K.J.; Henkel, C. The bursting nature of star formation in compact star-forming galaxies from the Sloan Digital Sky Survey. *Mon. Not. R. Astron. Soc.* **2016**, *462*, 4427–4434. [CrossRef]
5. Simon, J.D. The faintest dwarf galaxies. *Annu. Rev. Astron. Astrophys.* **2019**, *57*, 375–415. [CrossRef]

6. Minchin, R.F.; Disney, M.J.; Parker, Q.A.; Boyce, P.J.; de Blok, W.J.G.; Banks, G.D.; Ekers, R.D.; Freeman, K.C.; Garcia, D.A.; Gibson, B.K.; et al. The cosmological significance of low surface brightness galaxies found in a deep blind neutral hydrogen survey. *Mon. Not. R. Astron. Soc.* **2004**, *355*, 1303–1314. [CrossRef]
7. Nieto, J.L.; Bender, R.; Davoust, E.; Prugniel, P. The low-mass extension of the fundamental plane of elliptical galaxies. *Astron. Astrophys.* **1990**, *230*, L17–L20.
8. Aguerri, J.A.L.; González-García, A.C. On the origin of dwarf elliptical galaxies: The fundamental plane. *Astron. Astrophys.* **2009**, *494*, 891–904. [CrossRef]
9. Ferguson, H.C.; Binggeli, B. Dwarf elliptical galaxies. *Annu. Rev. Astron. Astrophys.* **1994**, *6*, 67–122. [CrossRef]
10. Jerjen, H.; Kalnajs, A.; Binggeli, B. IC3328: A dwarf elliptical galaxy wih spiral structure. *Astron. Astrophys.* **2000**, *358*, 845–849.
11. Barazza, F.D.; Binggeli, B.; Jerjen, H. More evidence for hidden spiral and bar features in bright early-type dwarf galaxies. *Astron. Astrophys.* **2002**, *391*, 823–831. [CrossRef]
12. De Rijcke, S.; Dejonghe, H.; Zeilinger, W.W.; Han, G.J.T. Embedded disks in Fornax dwarf elliptical galaxies. *Astron. Astrophys.* **2003**, *400*, 119–125. [CrossRef]
13. Henkel, C.; Wiklind, T. Cool dense gas in early-type galaxies. *Space Sci. Rev.* **1997**, *81*, 1–105. [CrossRef]
14. De Looze, I.; Baes, M.; Zibetti, S.; Fritz, J.; Cortese, L.; Davies, J.I.; Verstappen, J.; Bendo, G.J.; Bianchi, S.; Clemens, M.; et al. The Herschel Virgo Cluster survey: VII. Dust in cluster dwarf elliptical galaxies. *Astron. Astrophys.* **2010**, *518*, L54–L58. [CrossRef]
15. Tolstoy, E.; Hill, V.; Tosi, M. Star formationn histories, abundances, and kinematics of dwarf galaxies in the Local Group. *Annu. Rev. Astron. Astrophys.* **2009**, *47*, 371–425. [CrossRef]
16. Henkel, C.; Javanmardi, B.; Martínez-Delgado, D.; Kroupa, P.; Teuwen, K. DGSAT: Dwarf Galaxy Survey with Amateur Telescopes. II. A catalogue of isolated nearby edge-on disk galaxies and the discovery of new low surface brightness systems. *Astron. Astrophys.* **2017**, *603*, A18. [CrossRef]
17. Karachentsev, I.D.; Kaisina, E.I. Dwarf galaxies in the local volume. *Astrophys. Bull.* **2019**, *74*, 111–127. [CrossRef]
18. Cardamone, C.; Schawinski, K.; Sarzi, M.; Bamford, S.P.; Bennert, N.; Urry, C.M.; Lintott, C.; Keel, W.C.; Parejko, J.; Nichol, R.C.; et al. Galaxy zoo Green Peas: Discovery of a class of compact extremely star-forming galaxies. *Mon. Not. R. Astron. Soc.* **2009**, *399*, 1191–1205. [CrossRef]
19. Kormendy, J. Families of ellipsoidal stellar systems and the formation of dwarf elliptical galaxies. *Astrophys. J.* **1985**, *295*, 73–79. [CrossRef]
20. Jaiswal, S.; Omar, A. HI imaging of dwarf star-forming galaxies: Masses, morphologies, and gas deficiencies. *Mon. Not. R. Astron. Soc.* **2020**, *498*, 4745–4789. [CrossRef]
21. Richer, M.G.; Bullejos, A.; Borissova, J.; McCall, M.L.; Lee, H.; Kurtev, R.; Georgiev, L.; Kingsburgh, R.L.; Ross, R.; Rosado, M. IC 10: More evidence that it is a blue compact dwarf. *Astron. Astrophys.* **2001**, *370*, 34–42. [CrossRef]
22. Binggeli, B.; Sandage, A.; Tammann, G.A. Studies of the Virgo cluster. II. A catalog of 2096 galaxies in the Virgo cluster area. *Astron. J.* **1985**, *90*, 1681–1758. [CrossRef]
23. Guseva, N.G.; Papaderos, P.; Meyer, H.T.; Izotov, Y.I.; Fricke, K.J. An investigation of the luminosity-metallicity relation for a large sample of low-metallicity emission-line galaxies. *Astron. Astrophys.* **2009**, *505*, 63–72. [CrossRef]
24. Tremonti, C.A.; Heckman, T.M.; Kauffmann, G.; Brinchmann, J.; Charlot, S.; White, S.D.; Seibert, M.; Peng, E.W.; Schlegel, D.J.; Uomoto, A.; et al. The origin of the mass-metallicity relation: Insights from 53000 star-forming galaxies in the Sloan Digital Sky Survey. *Astrophys. J.* **2004**, *613*, 898–913. [CrossRef]
25. Gonçalves, T.S.; Basu-Zych, A.; Overzier, R.A.; Pérez, L.; Martin, D.C. Molecular gas properties of UV bright star-forming galaxies at low redshift. *Mon. Not. R. Astron. Soc.* **2014**, *442*, 1429–1439. [CrossRef]
26. Izotov, Y.I.; Guseva, N.G.; Fricke, K.J.; Henkel, C. On the universality of luminosity-metallicity and mass-metallicity relations for compact star-forming galaxies at redshifts $0 < z < 3$. *Mon. Not. R. Astron. Soc.* **2015**, *451*, 2251–2262.
27. Roychowdhury, S.; Chengalur, J.N.; Karachentsev, I.D.; Kaisina, E.I. The intrinsic shape of dwarf galaxies. *Mon. Not. R. Astron. Soc.* **2013**, *436*, L104–L108. [CrossRef]
28. Mateo, M.L. Dwarf galaxies of the Local Group. *Annu. Rev. Astron. Astrophys.* **1998**, *36*, 435–506. [CrossRef]
29. Socas-Navarro, H. The solar oxygen abundance from an empirical three dimensional model. *Astron. Astrophys.* **2015**, *577*, A25. [CrossRef]
30. Pilyugin, L.S.; Contini, T.; Vilchez, J.M. Chemical abundances in spiral and irregular galaxies. O and N abundances derived from global emission-line spectra. *Astron. Astrophys.* **2004**, *423*, 427–440. [CrossRef]
31. Pilyugin, L.S.; Vílchez, J.M.; Thuan, T.X. New improved calibration relations for the determination of electron temperatures and oxygen and nitrogen abundances in HII Regions. *Astron. Astrophys.* **2010**, *720*, 1738–1751.
32. Guseva, N.G.; Izotov, Y.I.; Stasínska, G.; Fricke, K.J.; Henkel, C.; Papaderos, P. VLT spectroscopy of low-metallicity emission-line galaxies: Abundance patterns and abundance discrepancies. *Astron. Astrophys.* **2011**, *529*, A149. [CrossRef]
33. Izotov, Y.I.; Stasińska, G.; Guseva, N.G.; Thuan, T.X. Abundance patterns in the low-metallicity emission-line galaxies from the Early Data Release of the Sloan Digital Sky Survey. *Astron. Astrophys.* **2004**, *415*, 87–94. [CrossRef]
34. Izotov, Y.I.; Thuan, T.X. Systematic effects and a new determination of the primordial abundance of ^{4}He and dY/dZ from observations of Blue Compact Galaxies. *Astrophys. J.* **2004**, *602*, 200–230. [CrossRef]
35. Izotov, Y.I.; Thuan, T.X. MMT observations of new extremely metal-poor emission-line galaxies in the Sloan Digital Sky Survey. *Astrophys. J.* **2007**, *665*, 1115–1128. [CrossRef]

36. Guseva, N.G.; Izotov, Y.I.; Papaderos, P.; Fricke, K.J. Balmer jump temperature determination in a large sample of low-metallicity HII regions. *Astron. Astrophys.* **2007**, *464*, 885–893. [CrossRef]
37. Begum, A.; Chengalur, J.N.; Karachentsev, I.D.; Sharina, M.E.; Kaisin, S.S. FIGGS: Faint irregular galaxies GMRT survey-overview, observations and first results. *Mon. Not. R. Astron. Soc.* **2008**, *386*, 1667–1682. [CrossRef]
38. Walter, F.; Brinks, E.; de Blok, W.J.G.; Bigiel, F.; Kennicutt, R.C.; Thornley, M.D.; Leroy, A. THINGS: The HI nearby galaxy survey, *Astron. J.* **2008**, *136*, 2563–2647.
39. Cannon, J.M.; Giovanelli, R.; Haynes, M.P.; Janowiecki, S.; Parker, A.; Salzer, J.J.; Adams, E.A.K.; Engstrom, E.; Huang, S.; McQuinn, K.B.W. The survey of HI in extremely low-mass dwarfs (SHIELD). *Astrophys. J.* **2011**, *739*, L22. [CrossRef]
40. Ott, J.; Stilp, A.M.; Warren, S.R.; Skillman, E.D.; Dalcanton, J.J.; Walter, F.; de Blok, W.J.G.; Koribalski, B.; West, A.A. *VLA*-ANGST: A high-resolution HI survey of nearby dwarf galaxies. *Astron. J.* **2012**, *144*, 123. [CrossRef]
41. Hunter, D.A.; Ficut-Vicas, D.; Ashley, T.; Brinks, E.; Cigan, P.; Elmegreen, B.G.; Heesen, V.; Herrmann, K.A.; Johnson, M.; Oh, S.-H.; et al. Little Things. *Astron. J.* **2012**, *144*, 134. [CrossRef]
42. MacHattie, J.A.; Irwin, J.A.; Madden, S.C.; Cormier, D.; Rémy-Ruyer, A. Detection of HI absorption in the dwarf galaxy Haro 11. *Mon. Not. R. Astron. Soc.* **2014**, *438*, L66–L70. [CrossRef]
43. Murthy, S.; Morganti, R.; Oosterloo, T.; Maccagni, F.M. The HI absorption zoo: JVLA extension to $z \sim 0.4$. *Astron. Astrophys.* **2021**, *654*, A94. [CrossRef]
44. Thuan, T.X.; Goehring, K.M.; Hibbard, J.E.; Izotov, Y.I.; Hunt, L.K. The HI content of extremely metal-deficient blue compact dwarf galaxies. *Mon. Not. R. Astron. Soc.* **2016**, *463*, 4268–4286. [CrossRef]
45. Ashley, T.; Simpson, C.E.; Elmegreen, B.G.; Johnson, M.; Pokhrel, N.R. The HI chronicles of Little Things BCDs. III. Gas clouds in and around Mrk 178, VII Zw 403, and NGC 3738. *Astron. J.* **2017**, *153*, 132. [CrossRef]
46. Kanekar, N.; Ghosh, T.; Rhoads, J.; Malhotra, S.; Harish, S.; Chengalur, J.N.; Jones, K.M. The atomic gas mass of Green Pea galaxies. *Astrophys. J.* **2021**, *913*, L15. [CrossRef]
47. Galliano, F.; Galametz, M.; Jones, A.P. The interstellar dust properties of nearby galaxies. *Annu. Rev. Astron. Astrophys.* **2018**, *56*, 673–713. [CrossRef]
48. Madden, S.C.; Cormier, D. Dwarf galaxies: Their low metallicity interstellar medium. *Proc. Int. Astron. Union* **2019**, *344*, 240–254. [CrossRef]
49. Feldmann, R. The equilibrium view on dust and metals in galaxies: Galactic outflows drive low dust-to-metal ratios in dwarf galaxies. *Mon. Not. R. Astron. Soc.* **2015**, *449*, 3274–3292. [CrossRef]
50. Lebouteiller, V.; Heap, S.; Hubeny, I.; Kunth, D. Chemical enrichment and physical conditions in IZw 18. *Astron. Astrophys.* **2013**, *553*, A16. [CrossRef]
51. Hunt, L.K.; Testi, L.; Casasola, V.; García-Burillo, S.; Combes, F.; Nikutta, R.; Caselli, P.; Henkel, C.; Maiolino, R.; Menten, K.M.; et al. ALMA observations of cool dust in a low-metallicity starburst, SBS 0335–052. *Astron. Astrophys.* **2014**, *561*, A49. [CrossRef]
52. w Rémy-Ruyer, A.; Madden, S.C.; Galliano, F.; Galametz, M.; Takeuchi, T.T.; Asano, R.S.; Zhukovska, S.; Lebouteiller, V.; Cormier, D.; Jones, A.; et al. Gas-to-dust mass ratios in local galaxies over a 2 dex metallicity range. *Astron. Astrophys.* **2014**, *563*, A31. [CrossRef]
53. Engelbracht, C.W.; Rieke, G.H.; Gordon, K.D.; Smith, J.-D.T.; Werner, M.W.; Moustakas, J.; Willmer, C.N.A.; Vanzi, L. Metallicity effects on dust prperties in starbursting galaxies. *Astrophys. J.* **2008**, *678*, 804–827. [CrossRef]
54. Rosenberg, J.L.; Wu, Y.; Le Floc'h, E.; Charmandaris, V.; Ashby, M.L.N.; Houck, J.R.; Salzer, J.J.; Willner, S.P. Dust properties and star formation rates in star-forming dwarf galaxies. *Astrophys. J.* **2008**, *674*, 814–830. [CrossRef]
55. Madden, S.C.; Rémy-Ruyer, A.; Galametz, M.; Cormier, D.; Lebouteiller, V.; Galliano, F.; Hony, S.; Bendo, G.J.; Smith, M.W.L.; Pohlen, M.; et al. An overview of the dwarf galaxy survey. *Publ. Astron. Soc. Pac.* **2013**, *125*, 600–635. [CrossRef]
56. Rémy-Ruyer, A.; Madden, S.C.; Galliano, F.; Hony, S.; Sauvage, M.; Bendo, G.J.; Roussel, H.; Pohlen, M.; Smith, M.W.L.; Galametz, M.; et al. Revealing the cold dust in low-metallicity environments. I. Photometry analysis of the Dwarf Galaxy Survey with *Herschel*. *Astron. Astrophys.* **2013**, *557*, A95. [CrossRef]
57. Rémy-Ruyer, A.; Madden, S.C.; Galliano, F.; Lebouteiller, V.; Baes, M.; Bendo, G.J.; Boselli, A.; Ciesla, L.; Cormier, D.; Cooray, A.; et al. Linking dust emission to fundamental properties in galaxies: The low-metallicity picture. *Astron. Astrophys.* **2015**, *582*, A121. [CrossRef]
58. Izotov, Y.I.; Guseva, N.G.; Fricke, K.J.; Henkel, C. Multi-wavelength study of 14000 star-forming galaxies from the Sloan Digital Sky Survey. *Astron. Astrophys.* **2014**, *561*, A33. [CrossRef]
59. Thuan, T.X.; Hunt, L.K.; Izotov, Y.I. The *Spitzer* view of low-metallicity star formation. II. Mrk996, a blue compact galaxy with an extremely dense nucleus. *Astrophys. J.* **2008**, *689*, 897–912. [CrossRef]
60. Izotov, Y.I.; Guseva, N.G.; Fricke, K.J.; Papaderos, P. SBS 0335–052 E+W: Deep VLT/FORS+UVES spectroscopy of the pair of the lowest metallicity blue compact dwarf galaxies. *Astron. Astrophys.* **2009**, *503*, 61–72. [CrossRef]
61. Izotov, Y.I.; Guseva, N.G.; Fricke, K.J.; Henkel, C. VLT/X-shooter observations of the low-metallicity blue compact dwarf galaxy PHL 293B, including a luminous blue variable star. *Astron. Astrophys.* **2011**, *533*, A25. [CrossRef]
62. Draine, B.T.; Li, A. Infrared emission from interstellar dust. IV. The silicate-graphit-PAH model in the post-*Spitzer* era. *Astrophys. J.* **2007**, *657*, 810–837. [CrossRef]
63. Bot, C.; Ysard, N.; Paradis, D.; Bernard, J.P.; Lagache, G.; Israel, F.P.; Wall, W.F. Submillimeter to centimeter excess emission from the Magellanic Clouds. II. On the nature of the excess. *Astron. Astrophys.* **2010**, *524*, A20. [CrossRef]

64. Galametz, M.; Madden, S.C.; Galliano, F.; Hony, S.; Bendo, G.J.; Sauvage, M. Probing the dust properties of galaxies up to the submillimetre wavelengths. II. Dust-to-gas mass ratio trends with metallicity and the submm excess in dwarf galaxies. *Astron. Astrophys.* **2011**, *532*, A56. [CrossRef]
65. Galliano, F.; Hony, S.; Bernard, J.-P.; Bot, C.; Madden, S.C.; Roman-Duval, J.; Galametz, M.; Li, A.; Meixner, M.; Engelbracht, C.W.; et al. Non-standard grain properties, dark gas reservoir, and extended submillimeter excess, probed by *Herschel* in the Large Magellanic Cloud. *Astron. Astrophys.* **2011**, *536*, A88. [CrossRef]
66. Dale, D.A.; Aniano, G.; Engelbracht, C.W.; Hinz, J.L.; Krause, O.; Montiel, E.J.; Roussel, H.; Appleton, P.N.; Armus, L.; Beirão, P.; et al. *Herschel* far-infrared and submillimeter photometry for the KINGFISH sample of nearby galaxies. *Astrophys. J.* **2012**, *745*, 95. [CrossRef]
67. Izotov, Y.I.; Guseva, N.G.; Fricke, K.J.; Krügel, E.; Henkel, C. Dust emission in star-forming dwarf galaxies: General properties and the nature of the submm excess. *Astron. Astrophys.* **2014**, *570*, A97. [CrossRef]
68. Galliano, F.; Madden, S.C.; Jones, A.P.; Wilson, C.D.; Bernard, J.-P.; Le Peintre, F. ISM properties in low-metallicity environments. II. The dust spectral energy distribution of NGC 1569. *Astron. Astrophys.* **2003**, *407*, 159–176. [CrossRef]
69. Galliano, F.; Madden, S.C.; Jones, A.P.; Wilson, C.D.; Bernard, J.-P. ISM properties in low-metallicity environments. III. The spectral energy distributions of II Zw 40, He 2–10 and NGC 1140. *Astron. Astrophys.* **2005**, *434*, 867–885. [CrossRef]
70. Hirashita, H. Properties of free-free, dust and CO emissions in the starbursts of blue compact dwrf galaxies. *Mon. Not. R. Astron. Soc.* **2013**, *429*, 3390–3401. [CrossRef]
71. Rubio, M.; Garay, G.; Montani, J.; Thaddeus, P. A ^{12}CO survey of the Small Magellanic Cloud. *Astron. Astrophys.* **1991**, *368*, 173–177.
72. Bolatto, A.D.; Wolfire, M.; Leroy, A.K. The CO-to-H_2 conversion factor. *Annu. Rev. Astron. Astrophys.* **2013**, *51*, 207–268. [CrossRef]
73. Amorín, R.; Muñoz-Tuñón, C.; Aguerri, J.A.L.; Planesas, P. Molecular gas in low-metallicity starburst galaxies: Scaling relation and the CO-to-H_2 conversion factor. *Astron. Astrophys.* **2016**, *588*, A23. [CrossRef]
74. Hunt, L.K.; García-Burillo, S.; Casasola, V.; Caselli, P.; Combes, F.; Henkel, C.; Lundgren, A.; Maiolino, R.; Menten, K.M.; Testi, L.; et al. Molecular depletion times and the CO-to-H_2 conversion factor in metal-poor galaxies. *Astron. Astrophys.* **2015**, *583*, A114. [CrossRef]
75. Wolfire, M.G.; Hollenbach, D.; McKee, C.F. The dark molecular gas. *Astrophys. J.* **2010**, *716*, 1191–1207. [CrossRef]
76. Rubio, M.; Lequeux, J.; Boulanger, F. Results from the ESO-SEST key programme: CO in the Magellanic Clouds. III. Molecular gas in the Small Magellanic Cloud. *Astron. Astrophys.* **1993**, *271*, 9–17.
77. Schruba, A.; Leroy, A.K.; Kruijssen, J.M.D.; Bigiel, F.; Bolatto, A.D.; de Blok, W.J.G.; Tacconi, L.; van Dishoeck, E.F.; Walter, F. Physical properties of molecular clouds at 2 pc resolution in the low-metallicity dwarf galaxy NGC 6822 and the Milky Way. *Astrophys. J.* **2017**, *835*, 278. [CrossRef]
78. Rich, J.; Persson, S.E.; Freedman, W.L.; Madore, B.F.; Monson, A.J.; Scowcroft, V.; Seibert, M. A new Cepheid distance measurement and method for NGC 6822. *Astrophys. J.* **2014**, *794*, 107. [CrossRef]
79. Rubio, M.; Elmegreen, B.G.; Hunter, D.A.; Brinks, E.; Cortés, J.R.; Cigan, P. Dense cloud cores revealed by CO in the low metallicity galaxy WLM. *Nature* **2015**, *525*, 218–221. [CrossRef]
80. Tammann, G.A.; Reindl, B.; Sandage, A. New period-luminosity and period-color relations of classical Cepheids. IV. The low-metallicity galaxies IC 1613, WLM, Pegasus, Sextans A and B, and Leo A in comparison to SMC. *Astron. Astrophys.* **2011**, *531*, A134. [CrossRef]
81. Shi, Y.; Wang, J.; Zhang, Z.-Y.; Zhang, Q.; Gao, Y.; Zhou, L.; Gu, Q.; Qiu, K.; Xia, X.-Y.; Hao, C.-N.; et al. Oversized gas clumps in an extremely metal-poor molecular cloud revealed by ALMA's parsec-scale maps. *Astrophys. J.* **2020**, *892*, 147. [CrossRef]
82. Kepley, A.A.; Leroy, A.K.; Johnson, K.E.; Sandstrom, K.; Chen, C.-H.R. The molecular clouds fueling a 1/5 solar metallicity starburst. *Astrophys. J.* **2016**, *828*, 50. [CrossRef]
83. Oey, M.S.; Herrera, C.N.; Silich, S.; Reiter, M.; James, B.L.; Jaskot, A.E.; Micheva, G. Dense CO in Mrk 71-A: Superwind supressed in a young super star cluster. *Astrophys. J.* **2017**, *849*, L1. [CrossRef]
84. Schneider, R.; Hunt, L.; Valiante, R. The dust content of the most metal-poor star-forming galaxies. *Mon. Not. R. Astron. Soc.* **2016**, *457*, 1842–1850. [CrossRef]
85. Klein, U.; Lisenfeld, U.; Verley, S. Radio synchrotron spectra of star-forming galaxies. *Astron. Astrophys.* **2018**, *611*, A55. [CrossRef]
86. Green, D.A. A catalogue of 294 galactic supernova remnants. *Bull. Astron. Soc. India* **2014**, *42*, 47–58. [CrossRef]
87. Thuan, T.X.; Izotov, Y.I. High-ionization emission in metal-deficient blue compact dwarf galaxies. *Astrophys. J. Suppl. Ser.* **2005**, *161*, 240–270. [CrossRef]
88. Izotov, Y.I.; Thuan, T.X.; Privon, G. The detection of [NeV] emission in five blue compact dwarf galaxies. *Mon. Not. R. Astron. Soc.* **2012**, *427*, 1229–1237. [CrossRef]
89. Izotov, Y.I.; Thuan, T.X.; Guseva, N.G. Large Binocular Telescope observations of new six compact star-forming galaxies with [NeV]λ3426 emission. *Mon. Not. R. Astron. Soc.* **2021**, *508*, 2556–2574. [CrossRef]
90. Kerp, J.; Walter, F.; Brinks, E. *ROSAT* X-ray observations of the dwarf galaxy Holmberg II. *Astrophys. J.* **2002**, *571*, 809–817. [CrossRef]
91. Snaith, O.; Haywood, M.; DiMatteo, P.; Lehnert, M.D.; Combes, F.; Katz, D.; Gómez, A. Reconstructing the star formation history of the Milky Way disc(s) from chemical abundances. *Astron. Astrophys.* **2015**, *578*, A87. [CrossRef]

92. Fantin, N.J.; Côté, P.; McConnachie, A.W.; Bergeron, P.; Cuillandre, J.-C.; Dufour, P.; Gwyn, S.D.J.; Ibata, R.A.; Thomas, G.F. The mass and age distribution of halo dwarfs in the Canada-France imaging survey. *Astrophys. J.* **2021**, *913*, 30. [CrossRef]
93. McQuinn, K.B.W.; Skillman, E.D.; Dalcanton, J.J.; Dolphin, A.E.; Cannon, J.M.; Holtzman, J.; Weisz, D.R.; Williams, B.F. Observational constraints on the molecular gas content in nearby starburst dwarf galaxies. *Astrophys. J.* **2012**, *751*, 127. [CrossRef]
94. Weisz, D.R.; Dalcanton, J.J.; Williams, B.F.; Gilbert, K.M.; Skillman, E.D.; Seth, A.C.; Dolphin, A.E.; McQuinn, K.B.W.; Gogarten, S.M.; Holtzman, J.; et al. The ACS nearby galaxy survey treasury. VIII. The global star formation histories of 60 dwarf galaxies in the local volume. *Astrophys. J.* **2011**, *739*, 5. [CrossRef]
95. Shen, S.; Madau, P.; Conroy, C.; Governato, F.; Mayer, L. The baryon cycle of dwarf galaxies: Dark, bursty gas-rich polluters. *Astrophys. J.* **2014**, *792*, 99. [CrossRef]
96. Emami, N.; Siana, B.; Weisz, D.R.; Johnson, B.D.; Ma, X.; El-Badry, K. A closer look at bursty star formation with $L(\mathrm{H}\alpha)$ and $L(\mathrm{UV})$ distributions. *Astrophys. J.* **2019**, *881*, 71. [CrossRef]
97. Cignoni, M.; Sacchi, E.; Tosi, M.; Aloisi, A.; Cook, D.O.; Calzetti, D.; Lee, J.C.; Sabbi, E.; Thilker, D.A.; Adamo, A.; et al. Star formation histories of the LEGUS Dwarf Galaxies. III. The nonbursty nature of 23 star-forming dwarf galaxies. *Astrophys. J.* **2019**, *887*, 112. [CrossRef]
98. Roychowdhury, S.; Chengalur, J.N.; Chiboucas, K.; Karachentsev, I.D.; Tully, R.B.; Kaisin, S.S. Atomic hydrogen, star formation and feedback in the lowest mass blue compact dwarf galaxies. *Mon. Not. R. Astron. Soc.* **2012**, *426*, 665–672. [CrossRef]
99. Hirashita, H.; Hunt, L.K. The role of dust in 'active' and 'passive' low-metallicity star formation. *Astron. Astrophys.* **2004**, *421*, 555–570.
100. Hunt, L.K.; Thuan, T.X.; Izotov, Y.I.; Sauvage, M. The *Spitzer* view of low-metallicity star formation. III. Fine-structure lines, aromatic features, and molecules. *Astrophys. J.* **2010**, *712*, 164–187. [CrossRef]
101. Puche, D.; Westphal, D.; Brinks, E.; Roy, J.-R. Holmberg II: A laboratory for studying the violent interstellar medium. *Astron. J.* **1992**, *103*, 1841–1858. [CrossRef]
102. Martin, M.C. Catalogue of HI maps of galaxies I. *Astron. Astrophys. Suppl. Ser.* **1998**, *131*, 73–75. [CrossRef]
103. Walter, F.; Brinks, E. Holes and shells in the interstellar medium of the nearby dwarf galaxy IC 2574. *Astron. J.* **1999**, *118*, 273–301. [CrossRef]
104. Weisz, D.R.; Skillman, E.D.; Cannon, J.M.; Dolphin, A.E.; Kennicutt, R.C.; Lee, J.; Walter, F. Does stellar feedback create HI holes? A *Hubble Space Telescope/Very Large Array* study of Holmberg II. *Astrophys. J.* **2009**, *704*, 1538–1569. [CrossRef]
105. Mac Low, M.-M.; Ferrara, A. Starburst-driven mass loss from dwarf galaxies: Efficiency and metal ejection. *Astrophys. J.* **1999**, *513*, 142–155. [CrossRef]
106. Ott, J.; Walter, F.; Brinks, E. A *Chandra* X-ray survey of nearby dwarf starburst galaxies-II. Starburst properties and outflows. *Mon. Not. R. Astron. Soc.* **2005**, *358*, 1453–1471. [CrossRef]
107. Lopez, L.A.; Krumholz, M.R.; Bolatto, A.D.; Prochaska, X.; Ramirez-Ruiz, E. What drives the expansion of giant HII regions?: A study of stellar feedback in 30 Doradus. *Astrophys. J.* **2011**, *791*, 91. [CrossRef]
108. Lopez, L.A.; Krumholz, M.R.; Bolatto, A.D.; Prochaska, J.X.; Ramirez-Ruiz, E.; Castro, D. The role of stellar feedback in the dynamics of HII regions. *Astrophys. J.* **2014**, *795*, 121. [CrossRef]
109. Hunt, L.K.; Weiß, A.; Henkel, C.; Combes, F.; García-Burillo, S.; Casasola, V.; Caselli, P.; Lundgren, A.; Maiolino, R.; Menten, K. M.; et al. Physical conditions of the molecular gas in metal-poor galaxies. *Astron. Astrophys.* **2017**, *606*, A99. [CrossRef]
110. Fahrion, K.; Cormier, D.; Bigiel, F.; Hony, S.; Abel, N.P.; Cigan, P.; Csengeri, T.; Graf, U.U.; Lebouteiller, V.; Madden, S.C.; et al. Disentangling the ISM phases of the dwarf galaxy NGC 4214 using [CII] SOFIA/GREAT observations. *Astron. Astrophys.* **2017**, *599*, A9. [CrossRef]
111. Lebouteiller, V.; Péquignot, D.; Cormier, D.; Madden, S.; Pakull, M.W.; Kunth, D.; Galliano, F.; Chevance, M.; Heap, S.R.; Lee, M.-Y.; et al. Neutral gas heating by X-rays in primitive galaxies: Infrared observations of the blue compact dwarf IZw 18 with *Herschel*. *Astron. Astrophys.* **2017**, *602*, A45. [CrossRef]
112. Accurso, G.; Saintonge, A.; Catinella, B.; Cortese, L.; Davé, R.; Dunsheath, S.H.; Genzel, R.; Gracia-Carpio, J.; Heckman, T.M.; Jimmy; Kramer, C.; et al. Deriving a multivariate α(CO) conversion function using the [CII]/CO (1-0) ratio and its application to molecular gas scaling relations. *Mon. Not. R. Astron. Soc.* **2017**, *470*, 4750–4766. [CrossRef]
113. Madden, S.C.; Cormier, D.; Hony, S. Tracing the total molecular gas in galaxies: [CII] and the CO-dark gas. *Astron. Astrophys.* **2020**, *643*, A141. [CrossRef]
114. Roychowdhury, S.; Chengalur, J.N.; Shi, Y. Extended Schmidt law holds for faint dwarf irregular galaxies. *Astron. Astrophys.* **2017**, *608*, A24. [CrossRef]
115. Guseva, N.G.; Izotov, Y.I.; Fricke, K.J.; Henkel, C. The MgII λ2797, λ2803 emission in low-metallicity star-forming galaxies from the SDSS. *Astron. Astrophys.* **2013**, *555*, A90. [CrossRef]
116. Guseva, N.G.; Izotov, Y.I.; Fricke, K.J.; Henkel, C. MgII λ2797, λ2803 emission in a large sample of low-metallicity star-forming galaxies from SDSS DR14. *Astron. Astrophys.* **2019**, *624*, A21. [CrossRef]
117. Barth, A.J.; Greene, J.E.; Ho, L.C. Dwarf Seyfert 1 nuclei and the low-mass end of the M(BH)-σ relation. *Astrophys. J.* **2005**, *619*, L151–L154. [CrossRef]
118. Barth, A.J.; Greene, J.E.; Ho, L.C. Low-mass Seyfert 2 galaxies in the *Sloan Digital Sky Survey*. *Astron. J.* **2008**, *136*, 1179–1200. [CrossRef]

119. Xiao, T.; Barth, A.J.; Greene, J.E.; Ho, L.C.; Bentz, M.C.; Ludwig, R.R.; Jiang, Y. Exploring the low-mass end of the M(BH)-σ^* relation with active galaxies. *Astrophys. J.* **2011**, *739*, 28. [CrossRef]
120. Izotov, Y.I.; Thuan, T.X. Active Galactic Nuclei in four metal-poor dwarf emission-line galaxies. *Astrophys. J.* **2008**, *687*, 133–140. [CrossRef]
121. Izotov, Y.I.; Guseva, N.G.; Fricke, K.J.; Stasińska, G.; Henkel, C.; Papaderos, P. Tol 2240-384—A new low-metallicity AGN candidate. *Astron. Astrophys.* **2010**, *517*, A90. [CrossRef]
122. Baldassare, V.F.; Reines, A.E.; Gallo, E.; Greene, J.E. A ≈50,000 $M_\odot$ solar mass black hole in the nucleus of RGG 118. *Astrophys. J.* **2015**, *809*, L14. [CrossRef]
123. Ahn, C.P.; Seth, A.C.; den Brok, M.; Strader, J.; Baumgardt, H.; van den Bosch, R.; Chilingarian, I.; Frank, M.; Hilker, M.; McDermid, R.; et al. Detection of supermassive black holes in two Virgo ultracompact dwarf Galaxies. *Astrophys. J.* **2017**, *839*, 72.
124. Kobulnicky, H.A.; Martin, C.L. The diffuse and compact X-ray components of the starburst galaxy Henize 2–10. *Astrophys. J.* **2010**, *718*, 724–738. [CrossRef]
125. Reines, A.E.; Sivakoff, G.R.; Johnson, K.E.; Brogan, C.L. An actively accreting massive black hole in the dwarf starburst galaxy Henize 2–10. *Nature* **2011**, *470*, 66–68. [CrossRef] [PubMed]
126. Reines, A.E.; Reynolds, M.T.; Miller, J.M. Deep *Chandra* observations of the compact starburst galaxy Henize 2–10: X-Rays from the massive black hole. *Astrophys. J.* **2016**, *830*, L35. [CrossRef]
127. Kaaret, P.; Corbel, S.; Prestwich, A.H.; Zezas, A. Radio emission from an ultraluminous X-ray source. *Science* **2003**, *299*, 365–368. [CrossRef] [PubMed]
128. Simmonds, C.; Bauer, F.E.; Thuan, T.X.; Zotov, Y.I.; Stern, D.; Harrison, F.A. Do some AGN lack X-ray emission? *Astron. Astrophys.* **2016**, *596*, A64. [CrossRef]
129. Baldwin, J.A.; Phillips, M.M.; Terlevich, R. Classification parameters for the emission-line spectra of extragalactic objects. *Publ. Astron. Soc. Pac.* **1981**, *93*, 5–19. [CrossRef]
130. Reines, A.E.; Greene, J.E.; Geha, M. Dwarf galaxies with optical signatures of active massive black holes. *Astrophys. J.* **2013**, *775*, 116. [CrossRef]
131. Molina, M.; Reines, A.E.; Latimer, C.J.; Baldassare, V.; Salehirad, S. A sample of massive black holes in dwarf galaxies detected via [Fex] coronal line emission: Active galactic nuclei and/or tidal disruption events. *arXiv* **2021**, arXiv:2108.09307.
132. Melioli, C.; Brighenti, F.; D'Ercole, A. Galactic fountains and outflows in star-forming dwarf galaxies: Interstellar medium expulsion and chemical enrichment. *Mon. Not. R. Astron. Soc.* **2015**, *446*, 299–316. [CrossRef]
133. McQuinn, K.B.W.; Skillman, E.D.; Heilman, T.N.; Mitchell, N.P.; Kelley, T. Galactic outflows, star formation histories, and time-scales in starburst dwarf galaxies from STARBIRDS. *Mon. Not. R. Astron. Soc.* **2018**, *477*, 3164–3177. [CrossRef]
134. Emerick, A.; Bryan, G.L.; Mac Low, M.-M. Stellar radiation is critical for regulating star formation and driving outflows in low-mass dwarf galaxies. *Astrophys. J.* **2018**, *865*, L22. [CrossRef]
135. Christensen, C.R.; Davé, R.; Brooks, A.; Quinn, T.; Shen, S. Tracing outflowing metals in simulations of dwarf and spiral galaxies. *Astrophys. J.* **2018**, *867*, 142. [CrossRef]
136. Koudmani, S.; Sijacki, D.; Bourne,M.A.; Smith, M.C. Fast and energetic AGN-driven outflows in simulated dwarf galaxies. *Mon. Not. R. Astron. Soc.* **2019**, *484*, 2047–2066. [CrossRef]
137. Manzano-King, C.M.; Canalizo, G.; Sales, L.V. AGN-driven outflows in dwarf galaxies. *Astrophys. J.* **2019**, *884*, 54. [CrossRef]
138. Hogarth, L.; Amorín, R.; Vílchez, J.M.; Hägele, G.F.; Cardaci, M.; Pérez-Montero, E.; Firpo, V.; Jaskot, A.; Chávez, R. Chemodynamics of green pea galaxies—I. Outflows and turbulence driving the escape of ionizing photons and chemical enrichment. *Mon. Not. R. Astron. Soc.* **2020**, *494*, 3541–3561. [CrossRef]
139. Bohn, T.; Canalizo, G.; Veilleux, S.; Liu, W. Near-infrared coronal line observations of dwarf galaxies hosting AGN-driven outflows. *Astrophys. J.* **2021**, *911*, 70. [CrossRef]
140. Lanfranchi, G.A.; Hazenfratz, R.; Caproni, A.; Silk, J. Parametrizing the outflow from a central black hole in dwarf spheroidal galaxies: A 3D Hydrodynamic Simulation. *Astrophys. J.* **2021**, *914*, 32. [CrossRef]
141. Mamon, G.A.; Trevisan, M.; Thuan, T.X.; Gallazzim, A.; Davé, R. The frequency of very young galaxies in the local Universe-II. The view from SDSS spectra. *Mon. Not. R. Astron. Soc.* **2020**, *492*, 1791–1811. [CrossRef]
142. Trevisan, M.; Mamon, G.A.; Thuan, T.X.; Ferrari, F.; Pilyugin, L.S.; Ranjan, A. The properties and environment of very young galaxies in the local Universe. *Mon. Not. R. Astron. Soc.* **2021**, *502*, 4815–4841. [CrossRef]
143. Tweed, D.P.; Mamon, G.A.; Thuan, T.X.; Cattaneo, A.; Dekel, A.; Menci, N.; Calura, F.; Silk, J. The frequency of very young galaxies in the local Universe: I. A test for galaxy formation and cosmological models. *Mon. Not. R. Astron. Soc.* **2018**, *477*, 1427–1450. [CrossRef]
144. Guseva, N.G.; Izotov, Y.I.; Fricke, K.J.; Henkel, C. New candidates for extremely metal-poor emission-line galaxies in the SDSS/BOSS DR10. *Astron. Astrophys.* **2015**, *579*, A11. [CrossRef]
145. Izotov, Y.I.; Thuan, T.X.; Guseva, N.G.; Liss, S.E. J0811+4730: The most metal-poor star-forming dwarf galaxy known. *Mon. Not. R. Astron. Soc.* **2018**, *473*, 1956–1966. [CrossRef]
146. Izotov, Y.I.; Thuan, T.X.; Guseva, N.G. J1234+3901: An extremely metal-deficient compact star-forming dwarf galaxy at redshift 0.133. *Mon. Not. R. Astron. Soc.* **2019**, *483*, 5491–5498. [CrossRef]

147. Kojima, T.; Ouchi, M.; Rauch, M.; Ono, Y.; Nakajima, K.; Isobe, Y.; Fujimoto, S.; Harikane, Y.; Hashimoto, T.; Hayashi, M. Extremely metal-poor representatives explored by the Subaru Survey (EMPRESS). I. A successful machine-learning selection of metal-poor galaxies and the discovery of a Galaxy with $M_* < 10^6$ $M_\odot$ and 0.016 $Z_\odot$. *Astrophys. J.* **2020**, *898*, 142.
148. Fukui, Y.; Kawamura, A. Molecular clouds in nearby galaxies. *Annu. Rev. Astron. Astrophys.* **2010**, *48*, 547–580. [CrossRef]
149. Huchtmeier, W.K. The giant HI-envelope of the irregular galaxy IC 10. *Astron. Astrophys.* **1979**, *75*, 170–175.
150. Cohen, R.J. The unusual kinematics of the galaxy IC 10. *Mon. Not. R. Astron. Soc.* **1979**, *187*, 839–845. [CrossRef]
151. Shostak, G.S.; Skillman, E.D. Neutral hydrogen observations of the irregular galaxy IC 10. *Astron. Astrophys.* **1989**, *214*, 33–42.
152. Ashley, T.; Elmegreen, B.G.; Johnson, M.; Nidever, D.L.; Simpson, C.E.; Pokhrel, N.R. The HI chronicles of LITTLE THINGS BCDs II: The Origin of IC 10's HI structure. *Astron. J.* **2014**, *148*, 130. [CrossRef]
153. Namumba, B.; Carignan, C.; Foster, T.; Deg, N. HI observations of IC 10 with the DRAO synthesis telescope. *Mon. Not. R. Astron. Soc.* **2019**, *490*, 3365–3377. [CrossRef]
154. Wilcots, E.M.; Miller, B.W. The kinematics and distribution of HI in IC 10. *Astron. J.* **1998**, *116*, 2363–2394. [CrossRef]
155. Polles, F.L.; Madden, S.C.; Lebouteiller, V.; Cormier, D.; Abel, N.; Galliano, F.; Hony, S.; Karczewski, O.Ł.; Lee, M.-Y.; Chevance, M.; et al. Modeling ionized gas in low-metallicity environments: the Local Group dwarf galaxy IC 10. *Astron. Astrophys.* **2019**, *622*, A119. [CrossRef]
156. Klein, U.; Gräve, R.; Wielebinski, R. A survey of the distribution of λ = 2.8 cm radio continuum in nearby galaxies. III. A small sample of irregular and blue compact galaxies. *Astron. Astrophys.* **1983**, *117*, 332–342.
157. Henkel, C.; Wouterloot, J.G.A.; Bally, J. H_2O and OH maser emission from bright IRAS galaxies. *Astron. Astrophys.* **1986**, *155*, 193–199.
158. Becker, R.; Henkel, C.; Wilson, T.L.; Wouterloot, J.G.A. H_2O masers in nearby irregular galaxies. *Astron. Astrophys.* **1993**, *268*, 483–490.
159. Leroy, A.; Bolatto, A.; Walter, F.; Blitz, L. Molecular gas in the low-metallicity star-forming dwarf IC 10. *Astrophys. J.* **2006**, *643*, 825–843. [CrossRef]
160. Kepley, A.A.; Bittle, L.; Leroy, A.K.; Jiménez-Donaire, M.J.; Schruba, A.; Bigiel, F.; Gallagher, M.; Johnson, K.; Usero, A. Dense molecular gas in the nearby low-metallicity dwarf starburst galaxy IC 10. *Astrophys. J.* **2018**, *862*, 120. [CrossRef]
161. Marleau, F.R.; Noriega-Crespo, A.; Misselt, K.A.; Gordon, K.D.; Engelbracht, C.W.; Rieke, G.H.; Barmby, P.; Willner, S.P.; Mould, J.; Gehrz, R.D.; et al. Mapping and mass measurement of the cold dust in NGC 205 with *Spitzer*. *Astrophys. J.* **2006**, *646*, 929–938. [CrossRef]
162. Young, L.M.; Lo, K.Y. Molecular clouds in the dwarf elliptical galaxy NGC 205. *Astrophys. J.* **1996**, *464*, L59–L62. [CrossRef]
163. Young, L.M. Properties of molecular clouds in NGC 205. *Astron. J.* **2000**, *120*, 2460–2470. [CrossRef]
164. Valluri, M.; Ferrarese, L.; Merritt, D.; Joseph, C.L. The low end of the supermassive black hole mass function: Constraining the mass of a nuclear black hole in NGC 205 via stellar kinematics. *Astrophys. J.* **2005**, *628*, 137–152. [CrossRef]
165. Nguyen, D.D.; Seth, A.C.; Neumayer, N.; Iguchi, S.; Cappellari, M.; Strader, J.; Chomiuk, L.; Tremou, E.; Pacucci, F.; Nakanishi, K.; et al. Improved dynamical constraints on the masses of the central black holes in nearby low-mass early-type galactic nuclei and the first black hole determination for NGC 205. *Astrophys. J.* **2019**, *872*, 104. [CrossRef]
166. Pustilnik, S.A.; Brinks, E.; Thuan, T.X.; Lipovetsky, V.A.; Izotov, Y.I. VLA HI line observations of the extremely metal-poor Blue Compact Dwarf galaxy SBS 0335–052. *Astron. J.* **2001**, *121*, 1413–1424. [CrossRef]
167. Thuan, T.X.; Lecavelier des Etangs, A.; Izotov, Y.I. Abundances in the HI envelope of the extremely low metallicity Blue Compact Dwarf galaxy SBS 0335-052 from *Far Ultraviolet Spectroscopic Explorer* observations. *Astrophys. J.* **2005**, *621*, 269–277. [CrossRef]
168. Thompson, R.I.; Sauvage, M.; Kennicutt, R.C.; Engelbracht, C.; Vanzi, L.; Schneider, G. Super star clusters in SBS 0335–052. *Astrophys. J.* **2009**, *691*, 1068–1078. [CrossRef]
169. Cormier, D.; Bendo, G.J.; Hony, S.; Lebouteiller, V.; Madden, S.C.; Galliano, F.; Glover, S.C.O.; Klessen, R.S.; Abel, N.P.; Bigiel, F.; et al. New *ALMA* constraints on the star-forming interstellar medium at low metallicity: A 50 pc view of the blue compact dwarf galaxy SBS 0335–052. *Mon. Not. R. Astron. Soc.* **2017**, *468*, L87–L91. [CrossRef]
170. Reines, A.E.; Johnson, K.E.; Hunt, L.K. A new view of the super star clusters in the low metallicity galaxy SBS 0335–052. *Astron. J.* **2008**, *136*, 1415–1426. [CrossRef]
171. Leroy, A.; Cannon, J.; Walter, F.; Bolatto, A.; Weiß, A. The low CO content of the extremely metal-poor galaxy IZw 18. *Astrophys. J.* **2007**, *663*, 990–994. [CrossRef]
172. Östlin, G.; Mouhcine, M. A new infrared view of evolved stars in IZw 18. *Astron. Astrophys.* **2005**, *433*, 797–806. [CrossRef]
173. Aloisi, A.; Clementini, G.; Tosi, M.; Annibali, F.; Contreras, R.; Fiorentino, G.; Mack, J.; Marconi, M.; Musella, I.; Saha, A.; et al. IZw 18 Revisited with *HST* ACS and Cepheids: New Distance and Age. *Astrophys. J.* **2007**, *667*, L151–L154. [CrossRef]
174. Izotov, Y.I.; Chaffee, F.H.; Foltz, C.B.; Green, R.F.; Guseva, N.G.; Thuan, T.X. Helium abundance in the most metal-deficient blue compact galaxies: IZw 18 and SBS 0335–052. *Astrophys. J.* **1999**, *527*, 757–777. [CrossRef]
175. Zhou, L.; Shi, Y.; Zhang, Z.-Y.; Wang, J. Extremely weak CO emission in IZw 18. *Astron. Astrophys.* **2021**, *653*, L10. [CrossRef]
176. Izotov, Y.I.; Thuan, T.X. Deep Hubble Space Telescope ACS Observations of IZw 18: A Young Galaxy in Formation. *Astrophys. J.* **2004**, *616*, 768–782. [CrossRef]
177. Aloisi, A.; Savaglio, S.; Heckman, T.M.; Hoopes, C.G.; Leitherer, C.; Sembach, K.R. Abundances in the neutral interstellar medium of IZw 18 from Far Ultraviolet Spectroscopic Explorer observations. *Astrophys. J.* **2003**, *595*, 760–778. [CrossRef]

178. Hunt, L.K.; Dyer, K.K.; Thuan, T.X.; Ulvestad, J.S. The radio continuum of the metal-deficient blue compact dwarf galaxy SBS 0335–052. *Astrophys. J.* **2004**, *606*, 853–861. [CrossRef]
179. Cannon, J.M.; Walter, F.; Skillman, E.D.; van Zee, L. The nature of radio continuum emission at very low metallicity: Very Large Array observations of IZw 18. *Astrophys. J.* **2005**, *621*, L21–L24. [CrossRef]
180. Johnson, K.E.; Hunt, L.K.; Reines, A.E. Probing star formation at low metallicity: The radio emission of super star clusters in SBS 0335–052. *Astron. J.* **2009**, *137*, 3788–3799. [CrossRef]
181. Hunt, L.K.; Dyer, K.K.; Thuan, T.X. The radio continuum of the extremely metal poor blue compact dwarf galaxy IZw 18. *Astrophys. J.* **2005**, *436*, 837–844.
182. Westmoquette, M.S.; Gallagher, J.S.; de Poitiers, L. Ionized gas in the starburst core and halo of NGC 1140. *Mon. Not. R. Astron. Soc.* **2010**, *403*, 1719–1728. [CrossRef]
183. Hunter, D.A.; O'Connell, R.W.; Gallagher, J.S. *Hubble Space Telescope* images of the central star-forming region in NGC 1140. *Astron. J.* **1994**, *108*, 84–89. [CrossRef]
184. de Grijs, R.; Smith, L.J.; Bunker, A.; Sharp, R.G.; Gallagher, J.S.; Anders, P.; Lançon, A.; O'Connell, R.W.; Parry, I.R. CIRPASS near-infrared integral-field spectroscopy of massive star clusters in the starburst galaxy NGC 1140. *Mon. Not. R. Astron. Soc.* **2004**, *352*, 263–276. [CrossRef]
185. Moll, S.L.; Mengel, S.; de Grijs, R.; Smith, L.J.; Crowther, P.A. Cluster and nebular properties of the central star-forming region of NGC 1140. *Mon. Not. R. Astron. Soc.* **2007**, *382*, 1877–1888. [CrossRef]
186. Ott, J.; Henkel, C.; Staveley-Smith, L.; Weiß, A. First detection of ammonia in the Large Magellanic Cloud: The kinetic temperature of dense molecular cores in N159 W. *Astrophys. J.* **2010**, *710*, 105–111. [CrossRef]
187. Tang, X.D.; Henkel, C.; Chen, C.-H.R.; Menten, K.M.; Indebetouw, R.; Zheng, X.W.; Esimbek, J.; Zhou, J.J.; Yuan, Y.; Li, D.L.; et al. Kinetic temperature of massive star-forming molecular clumps measured with formaldehyde. II. The Large Magellanic Cloud. *Astron. Astrophys.* **2017**, *600*, A16. [CrossRef]
188. Tang, X.D.; Henkel, C.; Menten, K.M.; Gong, Y.; Chen, C.-H.R.; Li, D.L.; Lee, M.-Y.; Mangum, J.G.; Ao, Y.P.; Mühle, S.; et al. Kinetic temperature of massive star-forming molecular clumps measured with formaldehyde IV. The *ALMA* view of N113 and N159 W in the LMC. *Astron. Astrophys.* **2021**, *655*, A12. [CrossRef]
189. Humire, P.; Thiel, V.; Henkel, C.; Belloche, A.; Loison, J.-C.; Pillai, T.; Riquelme, D.; Wakelam, V.; Langer, N.; Hernández-Gómez, A.; et al. Sulphur and carbon isotopes towards Galactic centre clouds. *Astron. Astrophys.* **2020**, *642*, A222. [CrossRef]
190. Szücs, L.; Glover, S.G.O.; Klessen, R.S. The ^{12}CO/^{13}CO ratio in turbulent molecular clouds. *Mon. Not. R. Astron. Soc.* **2014**, *445*, 4055–4072. [CrossRef]
191. Monreal-Ibero, A.; Walsh, J.R.; Vílchez, J.M. The ionized gas in the central region of NGC 5253. 2D mapping of the physical and chemical properties. *Astron. Astrophys.* **2012**, *544*, A60. [CrossRef]
192. Miura, R.E.; Espada, D.; Hirota, A.; Nakanishi, K.; Bendo, G.J.; Sugai, H. *ALMA* observations toward the starburst dwarf galaxy NGC 5253. I. Molecular cloud properties and scaling relations. *Astrophys. J.* **2018**, *864*, 120. [CrossRef]
193. Turner, J.L.; Consiglio, S.M.; Beck, S.C.; Goss, W.M.; Ho, P.T.P.; Meier, D.S.; Silich, S.; Zhao, J.-H. *ALMA* detects CO(3-2) within a Super Star Cluster in NGC 5253. *Astrophys. J.* **2017**, *846*, 73. [CrossRef]
194. Beck, S.C.; Lacy, J.; Turner, J.L.; Liu, H.B.; Greathouse, T.; Consiglio, S.M.; Ho, P.T.P. Ionized gas in the NGC 5253 supernebula: High spatial and spectral resolution observations with the JVLA and TEXES. *Mon. Not. R. Astron. Soc.* **2020**, *497*, 1675–1683. [CrossRef]
195. Calzetti, D.; Johnson, K.E.; Adamo, A.; Gallagher, J.S.; Andrews, J.E.; Smith, L.J.; Clayton, G.C.; Lee, J.C.; Sabbi, E.; Ubeda, L.; et al. The brightest young star clusters in NGC 5253. *Astrophys. J.* **2015**, *811*, 75. [CrossRef]
196. Silich, S.; Tenorio-Tagle, G. Gas expulsion versus gas retention in young stellar clusters-II. Effects of cooling and mass segregation. *Mon. Not. R. Astron. Soc.* **2018**, *478*, 5112–5122. [CrossRef]
197. Izotov, Y.I.; Thuan, T.X.; Guseva, N.G. A new determination of the primordial He abundance using the HeI λ10830Å emission line: Cosmological implications. *Mon. Not. R. Astron. Soc.* **2014**, *445*, 778–793. [CrossRef]
198. Aver, E.; Olive, K.A.; Skillman, E.D. The effects of HeIλ10830 on helium abundance determinations. *J. Cosmol. Astropart. Phys.* **2015**, *2015*, 11. [CrossRef]
199. Peimbert, A.; Peimbert, M.; Luridiana, V. The primordial helium abundance and the number of neutrino families. *Rev. Mex. Astron. Astroph.* **2016**, *52*, 419–424.
200. Fernández, V.; Terlevich, E.; Díaz, A.I.; Terlevich, R. A Bayesian direct method implementation to fit emission line spectra: Application to the primordial He abundance determination. *Mon. Not. R. Astron. Soc.* **2019**, *487*, 3221–3238. [CrossRef]
201. Valerdi, M.; Peimbert, A.; Peimbert, M.; Sixtos, A. Determination of the primordial helium abundance based on NGC 346, an HII region of the Small Magellanic Cloud. *Astrophys. J.* **2019**, *876*, 98. [CrossRef]
202. Hsyu, T.; Cooke, R.J.; Prochaska, J.X.; Bolte, M. The PHLEK survey: A new determination of the primordial helium abundance. *Astrophys. J.* **2020**, *896*, 77. [CrossRef]
203. Kurichin, O.A.; Kislitsyn, P.A.; Klimenko, V.V.; Balashev, S.A.; Ivanchik, A.V. A new determination of the primordial helium abundance using the analyses of HII region spectra from SDSS. *Mon. Not. R. Astron. Soc.* **2021**, *502*, 3045–3056. [CrossRef]
204. Valerdi, M.; Peimbert, A.; Peimbert, M. Chemical abundances in seven metal-poor HII regions and a determination of the primordial helium abundance. *Mon. Not. R. Astron. Soc.* **2021**, *505*, 3624–3634. [CrossRef]

205. Guseva, N.G.; Izotov, Y.I.; Thuan, T.X. A spectroscopic study of a large sample of Wolf-Rayet galaxies. *Astrophys. J.* **2000**, *531*, 776–803. [CrossRef]
206. Lee, J.C.; Kennicutt, R.C.; Funes, S.J.J.G.; Sakai, S.; Akiyama, S. Dwarf galaxy starburst statistics in the local volume. *Astrophys. J.* **2009**, *692*, 1305–1320. [CrossRef]
207. Huang, S.; Haynes, M.P.; Giovanelli, R.; Brinchmann, J.; Stierwalt, S.; Neff, S.G. Gas, stars, and star formation in ALFALFA dwarf galaxies. *Astron. J.* **2012**, *143*, 133. [CrossRef]
208. Izotov, Y.I.; Guseva, N.G.; Fricke, K.J.; Henkel, C.; Schaerer, D.; Thuan, T.X. Low-redshift compact star-forming galaxies as analogues of high-redshift star-forming galaxies. *Astron. Astrophys.* **2021**, *646*, A138. [CrossRef]
209. Troncoso, P.; Maiolino, R.; Sommariva, V.; Cresci, G.; Mannucci, F.; Marconi, A.; Meneghetti, M.; Grazian, A.; Cimatti, A.; Fontana, A.; et al. Metallicity evolution, metallicity gradients, and gas fractions at $z \approx 3.4$, *Astron. Astrophys.* **2014**, *563*, A58. [CrossRef]
210. Du, X.; Shapley, A.E.; Tang, M.; Stark, D.P.; Martin, C.L.; Mobasher, B.; Topping, M.W.; Chevallard, J. Searching for $z > 6.5$ analogs near the peak of cosmic star formation. *Astrophys. J.* **2020**, *890*, 65. [CrossRef]
211. Endsley, R.; Behroozi, P.; Stark, D.P.; Williams, C.C.; Robertson, B.E.; Rieke, M.; Gottlöber, S.; Yepes, G. Clustering with *JWST*: Constraining galaxy host halo masses, satellite quenching efficiencies, and merger rates at $z = 4$–10. *Mon. Not. R. Astron. Soc.* **2020**, *493*, 1178–1196. [CrossRef]
212. Tang, M.; Stark, D.P.; Chevallard, J.; Charlot, S.; Endsley, R.; Congiu, E. Rest-frame UV spectroscopy of extreme [OIII] emitters at $1.3 < z < 3.7$: Toward a high-redshift UV reference sample for *JWST*. *Mon. Not. R. Astron. Soc.* **2021**, *501*, 3238–3257.
213. Patej, A.; Loeb, A. Detectability of Local Group dwarf galaxy analogues at high redshifts. *Astrophys. J.* **2015**, *815*, L28. [CrossRef]
214. Alexandroff, R.M.; Heckman, T.M.; Borthakur, S.; Overzier, R.; Leitherer, C. Indirect evidence for escaping ionizing photons in local Lyman Break Galaxy analogs. *Astrophys. J.* **2015**, *810*, 104. [CrossRef]
215. Robertson, B.E.; Ellis, R.S.; Furlanetto, S.R.; Dunlop, J.S. Cosmic reionization and early star-forming galaxies: A joint analysis of new constraints from *Planck* and the *Hubble Space Telescope*. *Astrophys. J.* **2015**, *802*, L19. [CrossRef]
216. Schaerer, D.; Izotov, Y.I.; Verhamme, A.; Orlitová, I.; Thuan, T.X.; Worseck, G.; Guseva, N.G. The ionizing photon production efficiency of compact $z \approx 0.3$ Lyman continuum leakers and comparison with high-redshift galaxies. *Astron. Astrophys.* **2016**, *591*, L8. [CrossRef]
217. Chisholm, J.; Orlitová, I.; Schaerer, D.; Verhamme, A.; Worseck, G.; Izotov, Y.I.; Thuan, T.X.; Guseva, N.G. Do galaxies that leak ionizing photons have extreme outflows? *Astron. Astrophys.* **2017**, *605*, A67. [CrossRef]
218. Verhamme, A.; Orlitová, I.; Schaerer, D.; Izotov, Y.I.; Worseck, G.; Thuan, T.X.; Guseva, N.G. Lyman-α spectral properties of five newly discovered Lyman continuum emitters. *Astron. Astrophys.* **2017**, *597*, A13. [CrossRef]
219. Izotov, Y.I.; Worseck, G.; Schaerer, D.; Guseva, N.G.; Thuan, T.X.; Fricke, K.J.; Verhamme, A.; Orlitová, I. Low-redshift Lyman continuum leaking galaxies with high [OIII]/[OII] ratios. *Mon. Not. R. Astron. Soc.* **2018**, *478*, 4851–4855. [CrossRef]
220. Izotov, Y.I.; Worseck, G.; Schaerer, D.; Guseva, N.G.; Chisholm, J.; Thuan, T.X.; Fricke, K.J.; Verhamme, A. Lyman continuum leakage from low-mass galaxies with $M_* < 10^8$ $M_\odot$. *Mon. Not. R. Astron. Soc.* **2021**, *503*, 1734–1752.
221. Ramambason, L.; Schaerer, D.; Stasińska, G.; Guseva, N.G.; Vílchez, J.M.; Amorín, R.; Morisset, C. Reconciling escape fractions and observed line emission in Lyman-continuum-leaking galaxies. *Astron. Astrophys.* **2020**, *644*, A21. [CrossRef]
222. Wang, B.; Heckman, T.M.; Amorín, R.; Borthakur, S.; Chisholm, J.; Ferguson, H.; Flury, S.; Giavalisco, M.; Grazian, A.; Hayes, M.; et al. The low-redshift Lyman-continuum Survey: [SII] deficiency and the leakage of ionizing radiation. *Astrophys. J.* **2021**, *916*, 3. [CrossRef]
223. Izotov, Y.I.; Thuan, T.X.; Guseva, N.G. J2229+2725: An extremely low metallicity dwarf compact star-forming galaxy with an exceptionally high [OIII]λ5007/[OII]λ3727 flux ratio of 53. *Mon. Not. R. Astron. Soc.* **2021**, *504*, 3996–4004. [CrossRef]
224. Schaerer, D.; Izotov, Y.I.; Nakajima, K.; Worseck, G.; Chisholm, J.; Verhamme, A.; Thuan, T.X.; de Barros, S. Intense [CIII]$\lambda\lambda$1907,1909 emission from a strong Lyman continuum emitting galaxy. *Astron. Astrophys.* **2018**, *616*, L14. [CrossRef]
225. Guseva, N.G.; Izotov, Y.I.; Schaerer, D.; Vílchez, J.M.; Amorín, R.; Pérez-Montero, E.; Iglesias-Páramo, J.; Verhamme, A.; Kehrig, C.; Ramambason, L. Properties of five $z \approx 0.3$–0.4 confirmed LyC leakers: *VLT*/XShooter observations. *Mon. Not. R. Astron. Soc.* **2020**, *497*, 4293–4310. [CrossRef]
226. Chisholm, J.; Gazagnes, S.; Schaerer, D.; Verhamme, A.; Rigby, J.R.; Bayliss, M.; Sharon, K.; Gladders, M.; Dahle, H. Accurately predicting the escape fraction of ionizing photons using rest-frame ultraviolet absorption lines. *Astron. Astrophys.* **2018**, *616*, A30. [CrossRef]
227. Chisholm, J.; Prochaska, J.X.; Schaerer, D.; Gazagnes, S.; Henry, A. Optically thin spatially resolved MgII emission maps the escape of ionizing photons. *Mon. Not. R. Astron. Soc.* **2020**, *498*, 2554–2574. [CrossRef]
228. Izotov, Y.I.; Schaerer, D.; Worseck, G.; Verhamme, A.; Guseva, N.G.; Thuan, T.X.; Orlitová, I.; Fricke, K.J. Diverse properties of Lyα emission in low-redshift compact star-forming galaxies with extremely high [OIII]/[OII] ratios. *Mon. Not. R. Astron. Soc.* **2020**, *491*, 468–482. [CrossRef]
229. Choi, Y.; Dalcanton, J.J.; Williams, B.F.; Skillman, E.D.; Fouesneau, M.; Gordon, K.D.; Sandstrom, K.M.; Weisz, D.R.; Gilbert, K.M. Mapping the escape fraction of ionizing photons using resolved stars: A much higher escape fraction for NGC 4214. *Astrophys. J.* **2020**, *902*, 54. [CrossRef]
230. Gazagnes, S.; Chisholm, J.; Schaerer, D.; Verhamme, A.; Izotov, Y. The origin of the escape of Lyman α and ionizing photons in Lyman continuum emitters. *Astron. Astrophys.* **2020**, *639*, A85. [CrossRef]

231. Gronke, M.; Bull, P.; Dijkstra, M. A systematic study of Lyman-α transfer through outflowing shells: Model parameter estimation. *Astrophys. J.* **2015**, *812*, 123. [CrossRef]
232. Matthee, J.; Sobral, D.; Gronke, M.; Paulino-Afonso, A.; Stefanon, M.; Röttgering, H. Confirmation of double peaked Lyα emission at $z = 6.593$. Witnessing a galaxy directly contributing to the reionisation of the Universe. *Astron. Astrophys.* **2018**, *619*, A136. [CrossRef]
233. Weisz, D.R.; Boylan-Kolchin, M. Local Group ultra-faint dwarf galaxies in the reionization era. *Mon. Not. R. Astron. Soc. Lett.* **2017**, *469*, L83–L88. [CrossRef]